Vol. 2 December, 1956 No. 1

MINERALOGICAL JOURNAL

CONTENTS

The Crystal Structure of Borax ..... N. Morimoto... 1

The Crystal Structure of Vonsenite ..... Y. Takéuchi...19

Chemical Studies of Lithium Micas from the Pegmatite of Minagi, Okayama Prefecture ..... Y. Ukai, S. Nishimura and Y. Hashimoto...27

Dependence of the Optical Absorption on the Crystallographic Orientation in Heikolite ..... T. Shoda...39

Short Communications

Frequency Distribution of the Composition of Plagioclases in Some Igneous Rocks ..... T. Sueno...48

Abstract of the Kobutsugaku Zasshi, Journal of the Mineralogical Society of Japan, Vol. 3, No. 1 59

The Mineralogical Society of Japan

Department of Geology and Mineralogy, Faculty of Science, Hokkaido University, Sapporo, Japan

MINERALOGICAL JOURNAL

published by

The Mineralogical Society of Japan

EDITORIAL BOARD

Zyunpei HARADA, *Hokkaido University;* Teiichi ITO, *University of Tokyo;* (Chief) Nobuo KATAYAMA, *University of Tokyo;* Keiichi OMORI, *Tohoku University;* Ryôiti KIRIYAMA, *University of Osaka;* Seitaro TSUBOI, *University of Tokyo;* Takeo WATANABE, *University of Tokyo;* Toyofumi YOSHIMURA, *Kyushu University.*

Instructions to Contributors

Manuscripts of articles should be submitted to the executive editor, Nobuo Katayama, at the College of General Education, University of Tokyo, Komaba, Meguro-ku, Tokyo. The manuscript should be type-written with double space lines, and not exceed 20 sheets of normal type-writing paper. References of literature should be in accordance with the forms used in the pages of this journal.

Plates and figures should be capable of reduction to not more than 10 by 15 centimetres. Line drawings should be in black India ink on white drawing board, tracing paper, or coordinate paper printed in blue. Photographs should be positive glossy prints.

Two referees chosen by the Editorial Board read the manuscript of article submitted before it is accepted for publication.

Thirty reprints without cover will be furnished to the author free of cost and without previous notice from him. Additional reprints will be furnished at cost when ordered.

The price of the journal to subscribers in Japan is 250 yen for a single copy (including postage), and to subscribers in other countries $ 1.00 (including postage) for a single copy, or $ 5.00 (including postage) per volume of 6 numbers.

Printed in Japan

MINERALOGICAL JOURNAL, VOL. 2, No. 1, pp. 1-18, DEC., 1956

THE CRYSTAL STRUCTURE OF BORAX*

NOBUO MORIMOTO

Mineralogical Institute, University of Tokyo

ABSTRACT

The crystal structure of borax, $Na_2B_4O_7 \cdot 10H_2O$, has been worked out by means of the sign relationships of structure factors and by the triple Fourier series method. The unit cell has the dimensions of $a_0=11.858$ Å, $b_0=10.674$ Å, $c_0=12.197$ Å and $\beta=106°41'$, and the space group is C_{2h}^6. There are four chemical units of composition, $Na_2B_4O_7 \cdot 10H_2O$ in the unit cell. The coordinates of atoms were refined first by double Fourier series and the final triple Fourier series were carried out with 1763 terms. The standard deviations of coordinates finally obtained are 0.004 Å for sodium atoms, 0.02 Å for boron atoms and 0.02 Å for oxygen atoms. Hydrogen atoms have been located from the consideration on the electrostatic valencies directed to the oxygen atoms and the interatomic distances between oxygen atoms.

The structure of borax is composed of chains of regular octahedra formed by water molecules around Na, running parallel to the c-axis. These chains build up a sheet holding isolated groups of $B_4O_5(OH)_4$ in between them through hydrogen bonds. These sheets are parallel to (100) and held together mainly by hydrogen bonds. The structure formula of borax may best be represented with the expression $B_4O_5(OH)_4 \cdot Na_28H_2O$.

Introduction

There have remained many problems unsolved concerning the crystal structures of borate minerals and their mutual relations, among which borax, $Na_2B_4O_7 \cdot 10H_2O$, is of most importance because of its practical use. In the present study, the crystal structure of borax was determined as part of a programme of investigation of the borate minerals at this Mineralogical Institute. The structure of this mineral is of special interest because of the possibility of finding the structural units of boron, oxygen and hydrogen atoms which or part of which might give clues to solve the structure of

* Read at the Annual Meeting of the Mineralogical Society of Japan held in Kyoto on Oct. 23, 1955.

other borate minerals and because of the role played in the structure by the hydrogen atoms.

Since no assumption was made about the location of hydrogen atoms in advance, and they are omitted in calculating the structure factors, the term "oxygen atom" throughout this paper will be used comprehensively to include O^{2-}, OH^- and H_2O groups, without distinguishing between them, except where context makes distinction obvious.

Only few X-ray studies on borax have so far been reported. W. Minder[8] gave, in 1935, the lattice constants and space group of borax with other kindred minerals such as kernite ($Na_2B_4O_7 \cdot 4H_2O$) and tincalconite ($Na_2B_4O_7 \cdot 5H_2O$). Recently, José Ma. Font Tullot[4][9] proposed its crystal structure on the basis of his X-ray data.

Experimental

As the material for this study, commercial borax was used after recrystallization. The lattice constants were determined first with the rotation photographs about the a-, b- and c-axes. The values obtained are $a_0=11.80\pm0.04$ Å, $b_0=10.67\pm0.05$ Å, $c_0=12.29\pm0.04$ Å and $\beta=106°35'$ (from goniometer measurement). At the later stage of the analysis, the redetermination of these values was carried out by the powder method with a "Norelco" X-ray diffractometer, quartz and silicon being chosen as the standard substances. The results obtained are $a_0=11.858\pm0.005$Å, $b_0=10.674\pm0.005$Å, $c_0=12.197\pm0.005$Å and $\beta=106°41'\pm2'$. In the unit cell, there are four chemical units of composition $Na_2B_4O_7 \cdot 10H_2O$. The space group is C_{2h}^6-C^2/c, (hkl) being present only when $h+k=2n$, ($h0l$) only when $h=2n$ and $l=2n$ and ($0k0$) only when $k=2n$. These results are in good agreement with the ones previously described[8][4].

Integrating Weissenberg photographs[10] were taken about the a-, b- and c-axes each up to the seventh layer by the multiple film technique. The samples used for this purpose were needle-crystals of about 0.5 mm.×0.5 mm. in cross section and 1 mm. in length.

Throughout the experiments, Cu$k\alpha$ radiation (λ=1.542 Å) was used.

The relative intensities were estimated visually and corrected for the Lorentz and polarization factors. No correction was made for absorption, nor for extinction. After the relative intensities were adjusted to the same scale, they were put on to the absolute ones by Willson's method[11], which gave B=1.40 Å^2 for the temperature factor parameter. At the later stage of the analysis, these absolute intensities were found to be less by about 5% than the values expected from the correct structure.

Analysis

Since no structure of hydrated sodium borates has so far been determined, it was impossible to assume beforehand the probable arrangement of atoms for this mineral from the structural view-point, and the usual trial and error method could not be effectively employed. Moreover, since this mineral has a number of comparatively light atoms such as sodium, oxygen, boron and hydrogen atoms in the large unit cell, the application of the Patterson function was not expected to be effective. Therefore, the only probable way of attacking the problem was to make use of the sign relationships of structure factors.

This method was first applied to the two-dimensional reflections, that is, F_{hk0}'s, F_{k0l}'s and F_{0kl}'s. It was, however, impossible to obtain signs of reflections enough to produce a comprehensible Fourier projection.

Then all the three-dimensional observed structure factors, F_{hkl}'s which amount to about 1800 including 681 absent ones, were used for the sign determination. Since the origin of the unit cell may be shifted from one symmetry centre to another, it is possible to choose the signs of two structure factors at will in the space group of borax, C_{2h}^6. Thus the positive sign was chosen for the reflections (170) and (735). It was found then that the signs of fifteen additional structure factors were uniquely determined from the following rela-

tion by Harker and Kasper[5],

$$(U_{h,k,l} \pm U_{h',k',l'})^2 \leqq (1 \pm U_{h+h',\, k+k',\, l+l'})(1 \pm U_{h-h',k-k',l-l'}).$$

On the basis of the known signs, Cochran's relation[2)3)], $S_H = S_K \cdot S_{H+K}$, was applied to all the structure factors whose U-values were more than 0.30. According to this procedure, the signs of 66 structure factors were expressed by +, − and two letter symbols a and b. For all the large structure factors not determined by the above methods and ones whose U-values were more than 0.20, Zachariasen's relationship[12)], $S_H = (\overline{S_K \cdot S_{H+K}})$, was tested, and the signs of additional 144 reflections, as well as of the letters a and b, were deduced from the known ones.

Up to this stage, therefore, the signs of comparatively large 225 structure factors had been collected and it was expected that a three-dimensional Fourier synthesis based on these factors would give a good approximation to the correct structure. The three-dimensional

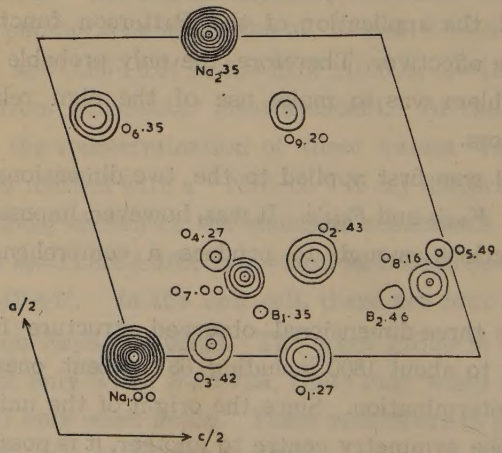

Fig. 1. The composite sections from $\rho(xyz)$ by the first triple Fourier series. The sections are projected on (010). The lower half only of $1/2a_0 \times 1/2c_0$ is shown. Contours are drawn at equal intervals of an arbitray scale. The numbers give the height of each atom expressed as a percentage of the b_0-translation.

Fourier summation was carried out over the points of 1/30×1/30×1/30 of the unit cell. The Beever-Lipson strips were used for the calculation according to the next equation,

$$\rho_{xyz}=\frac{4}{V_c}\sum_{k=0}^{\infty}(J_{kxz}\cos 2\pi ky-j_{kxz}\sin 2\pi ky),$$

where $$J_{kxz}=\sum_{h}\sum_{l}^{l=2n}[F_{hkl}\cos 2\pi(hx+lz)+F_{\bar{h}kl}\cos 2\pi(-hx+lz)]$$

and $$j_{kxz}=\sum_{h}\sum_{l}^{l=2n+1}[F_{hkl}\sin 2\pi(hx+lz)+F_{\bar{h}kl}\sin 2\pi(-hx+lz)].$$

The composite Fourier sections from $\rho(xyz)$ are given in Fig. 1, projected on to (010).

Since the heights of peaks at the centres of sodium, oxygen and boron atoms in the three-dimensional electron density map were expected to have the proportion of about 3 : 2 : 1 respectively as

Table 1. The atomic coordinates in borax.

Atoms	No. of atoms in the cell	Column 1			Column 2			Column 3		
		x/a_0	y/b_0	z/c_0	x/a_0	y/b_0	z/c_0	x/a_0	y/b_0	z/c_0
Na_1	4	0	0	0	0	0	0	0	0	0
Na_2	4	0	.847	.250	0	.843	.250	0	.845	.250
B_1	8	.080	.347	.213	.082	.347	.215	.085	.345	.217
B_2	8	.095	.460	.390	.098	.450	.397	.095	.454	.390
O_1	4	0	.273	.250	0	.264	.250	0	.265	.250
O_2	8	.143	.427	.305	.156	.420	.318	.154	.419	.314
O_3	8	.025	.430	.125	.021	.437	.123	.018	.435	.123
O_4	8	.158	.267	.170	.158*	.264	.167	.161	.269	.167
O_5	8	.162	.493	.495	.165	.493*	.495*	.163	.511	.491
O_6	8	.127	.850	.447	.123	.845	.453	.123	.846	.450
O_7	8	.127	0	.195	.121	.002	.192	.125	.002	.196
O_8	8	.117	.157	.462	.120	.163	.455	.119	.165	.459
O_9	8	.118	.700	.167	.118*	.705	.178	.116	.707	.171

Column 1: The coordinates from the first triple Fourier series.
Column 2: The coordinates after two-dimensional refinements.
Column 3: The final coordinates from the second triple Fourier series.

observed in other crystals, it was easy to allot two sodium, nine oxygen and two boron atoms to the appropriate peaks in the diagram of the unsymmetrical domain of the unit cell. The results thus derived produced a structure which showed no contradiction to the known crystallographic knowledge such as the ionic radii of atoms and the coordination number of cations. These first approximate coordinates of atoms are given in Table 1, column 1.

Refinement of coordinates

Two-dimensional Fourier methods were employed as far as possible to refine the atomic parameters. All the signs of observed F_{hk0}'s, F_{h0l}'s and F_{0kl}'s were derived from the above coordinates. Hartree's atomic scattering factors were used in this calculation with $B=1.40$ Å^2 for the temperature factor parameter. Two-dimensional Fourier diagrams projected on to (001), (010) and (100) were produced, the a-, b- and c-axes being divided into 60 parts. After several successive adjustments, all the signs ceased to change. The final coordinates of atoms whose peaks were resolved in the maps were given in Table 1, column 2. Throughout these processes, the original coordinates were used for oxygen atoms whose peaks overlapped in the maps and given in Table 1, column 2 with stars. The coordinates of boron atoms were adjusted in accordance with spatial requirements with oxygen atoms. The reliability factors based on these coordinates were 0.221 for F_{hk0}'s, 0.194 for F_{h0l}'s and 0.253 for F_{0kl}'s, all present and absent reflections being counted.

The structure factors of general reflections, F_{hkl}'s, were then calculated with these coordinates. After calculation, it was found that the originally observed F-values should be increased by 5% to obtain the least values for the reliability factors, which reduced from 0.240 to 0.231 including present and absent reflections. With the corrected values of observed F_{hkl}'s, the three-dimensional Fourier series were recalculated, each axis being divided into 30 parts as earlier. The composite Fourier sections from $\rho(xyz)$ are projected on (010) and

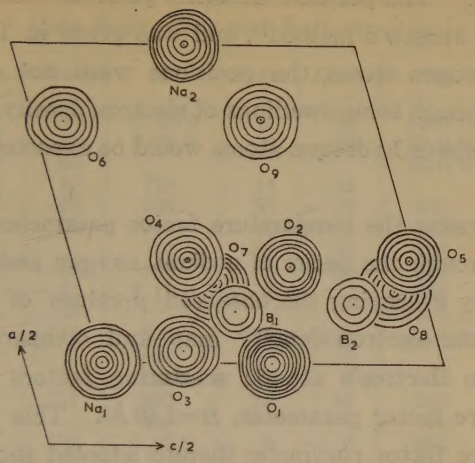

(a)

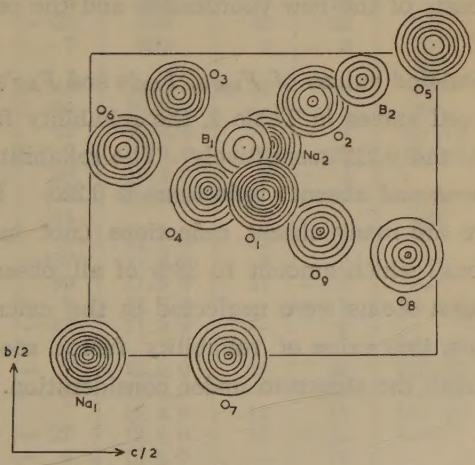

(b)

Fig. 2. The composite sections from ρ (xyz) by the second triple Fourier series. The sections are projected on (a) (010) and (b) (100). The lower halves only of $1/2a_0 \times 1/2c_0$ and $1/2c_0 \times 1/2b_0$ are shown in (a) and (b) respectively. Dots indicate positions of atoms according to the final parameters. Contours are drawn at 2, 4, 6.....*e.* Å^{-3} for boron and oxygen atoms and 2, 4, 8, 12,.....*e.* Å^{-3} for sodium atoms.

(100) in Fig. 2. The position of each peak in the diagram was determined by Megaw's method[7], and was given in Table 1, column 3. As for hydrogen atoms, the positions were not determined in the diagram, though some swellings of electron density were observed at the places where hydrogen atoms would be expected as mentioned below.

In order to refine the temperature factor parameter, at this stage, the profiles through the peaks of sodium, oxygen and boron atoms were plotted by averaging the observed ρ-values of atoms of the same kind in the electron density map and compared with those calculated from Hartree's atomic scattering factors modified with the temperature factor parameter, B=1.40 Å^2. This indicated that the temperature factor parameter thereto adopted should be increased to B=1.60 Å^2. The structure factors of F_{hkl}'s were calculated again on the basis of the new coordinates and the revised temperature factor.

Only the calculated values of F_{hk0}'s, F_{h0l}'s and $F_{h0\bar{l}}$'s are compared with the observed values in Table 2, the reliability factors of which are 0.190, 0.154, and 0.212 respectively. The reliability factor for all observed (present and absent) reflections is 0.220. In view of the facts that there are many absent reflections (not including space-group extinctions) which amount to 38% of all observed ones and that the hydrogen atoms were neglected in the calculation of the structure factors, this value of reliability factor seems to be sufficient to establish the structure under consideration.

Accuracy

In this work, systematic errors such as from extinction, absorption and termination effect in Fourier synthesis were not corrected. Therefore, in order to take accunt of these errors, the order of magniude of the standard deviation of atomic coordinates was estimated from the following expression,

Table 2. Comparison of observed and calculated F-values. Only F_{hk0}'s, F_{h0l}'s and F_{0kl}'s are given.

hkl	*F*obs.	*F*calc.	*hkl*	*F*obs.	*F*calc.	*hkl*	*F*obs.	*F*calc.
020	33	34	6.10.0	12	18	10.0.0	38	35
040	83	88	6.12.0	19	23	12.0.0	28	26
060	80	83				14.0.0	6	8
080	12	16	710	11	22			
0.10.0	12	21	730	22	− 19	002	37	− 34
0.12.0	38	50	750	30	31	202	54	− 53
			770	82	79	402	38	− 26
110	23	− 15	790	15	− 26	602	27	− 25
130	24	− 31	7.11.0	8	7	802	22	− 22
150	38	39				10.0.2	15	− 14
170	133	142	800	134	128	12.0.2	24	− 21
190	—	− 3	820	—	0			
1.11.0	31	29	840	12	8	004	90	90
1.13.0	11	11	860	38	44	204	163	211
			880	—	4	404	26	33
200	94	118	8.10.0	6	− 2	604	31	− 30
220	19	16				804	11	7
240	6	− 6	910	64	61	10.0.4	44	44
260	27	27	930	—	3	12.0.4	37	30
280	—	− 4	950	26	29			
2.10.0	20	− 20	970	50	53	006	98	92
2.12.0	10	7	990	9	8	206	21	− 14
						406	86	− 83
310	41	48	10.0.0	38	35	606	42	30
330	32	30	10.2.0	—	3	806	43	32
350	36	42	10.4.0	—	− 3	10.0.6	14	− 6
370	—	− 2	10.6.0	30	29	12.0.6	—	2
390	31	29	10.8.0	8	− 4			
3.11.0	—	6	10.10.0	—	− 17	008	—	3
3.13.0	—	14				208	87	86
			11.1.0	12	− 12	408	96	106
400	143	−157	11.3.0	6	2	608	24	22
420	27	30	11.5.0	11	− 5	808	—	− 5
440	8	− 9	11.7.0	—	− 3	10.0.8	27	32
460	43	− 42	11.9.9	—	9			
480	10	4				0.0.10	—	6
4.10.0	—	− 7	12.0.0	28	26	2.0.10	19	18
4.12.0	—	− 5	12.2.0	—	12	4.0.10	25	− 14
			12.4.0	14	15	6.0.10	29	− 18
510	26	− 27	12.6.0	12	− 12	8.0.10	18	− 16
530	—	− 9	12.8.0	—	11			
550	10	13				0.0.12	12	10
570	17	9	13.1.0	22	− 21			
590	—	1	13.3.0	6	4	2.0.12	12	10
5.11.0	8	− 6	13.5.0	—	1	4.0.12	6	17
			14.0.0	6	8	6.0.12	45	37
600	134	154				0.0.14	26	− 27
620	39	22	200	94	118	2.0.14	—	− 14
640	53	60	400	143	−157			
660	19	− 11	600	134	154	$20\bar{2}$	10	− 6
680	26	22	800	134	128	$40\bar{2}$	10	− 6
						$60\bar{2}$	16	8

$80\bar{2}$	19	15	061	—	0	067	29	28
$10.0.\bar{2}$	13	10	081	—	− 11	087	30	27
$12.0.\bar{2}$	—	− 5	0.10.1	—	14	0.10.7	—	− 2
$14.0.\bar{2}$	—	− 9	0.12.1	40	38	0.12.7	—	− 1
$20\bar{4}$	156	−158	002	37	− 34	008	—	3
$40\bar{4}$	—	− 4	022	83	91	028	42	46
$60\bar{4}$	140	160	042	12	− 8	048	28	24
$80\bar{4}$	74	69	062	87	76	068	—	8
$10.0.\bar{4}$	18	− 16	082	—	11	088	—	7
$12.0.\bar{4}$	—	4	0.10.2	—	10	0.10.8	—	− 10
$14.0.\bar{4}$	47	42	0.12.2	—	5			
						009	—	—
$20\bar{6}$	98	−102	003	—	—	029	—	− 4
$40\bar{6}$	68	− 76	023	22	19	049	22	13
$60\bar{6}$	62	64	043	62	− 59	069	—	− 2
$80\bar{6}$	60	− 45	063	16	− 22	089	—	− 2
$10.0.\bar{6}$	73	− 67	083	—	9	0.10.9	—	− 7
$12.0.\bar{6}$	—	2	0.10.3	—	− 4			
$14.0.\bar{6}$	—	− 3	0.12.3	—	− 2	0.0.10	—	6
						0.2.10	78	86
$20\bar{8}$	58	58	004	90	90	0.4.10	42	41
$40\bar{8}$	134	134	024	16	24	0.6.10	—	4
$60\bar{8}$	67	70	044	14	14	0.8.10	—	12
$80\bar{8}$	10	6	064	105	110	0.10.10	27	27
$10.0.\bar{8}$	34	30	084	62	58			
$12.0.\bar{8}$	47	52	0.10.4	—	8	0.0.11	—	—
$14.0.\bar{8}$	20	23	0.12.4	36	37	0.2.11	—	− 2
						0.4.11	31	− 26
$2.0.\bar{10}$	40	− 46	005	—	—	0.6.11	—	− 11
$4.0.\bar{10}$	—	7	025	8	− 20	0.8.11	—	6
$6.0.\bar{10}$	31	33	045	70	58			
$8.0.\bar{10}$	10	− 13	065	31	34	0.0.12	12	10
$10.0.\bar{10}$	—	− 12	085	15	− 24	0.2.12	12	− 14
$12.0.\bar{10}$	18	22	0.10.5	—	− 9	0.4.12	36	36
$14.0.\bar{10}$	—	13	0.12.5	—	6	0.6.12	—	− 8
						0.8.12	22	20
$2.0.\bar{12}$	10	− 6	006	98	92			
$4.0.\bar{12}$	31	34	026	47	46	0.0.13	—	—
$6.0.\bar{12}$	49	41	046	85	93	0.2.13	—	5
$8.0.\bar{12}$	—	− 6	066	—	1	0.4.13	—	− 5
$10.0.\bar{12}$	25	25	086	18	15	0.6.13	—	0
$12.0.\bar{12}$	35	46	0.10.6	56	52			
$14.0.\bar{12}$	—	− 13	0.12.6	—	9	0.0.14	26	− 27
001	—	—	007	—	—	0.2.14	18	12
021	107	−128	027	34	34	0.4.14	—	10
041	48	− 48	047	19	− 21			

$$\sigma(x)=-\sigma\left(\frac{\partial\rho}{\partial x}\right)\Big/\left(\frac{\partial^2\rho}{\partial x^2}\right)_{\text{Peak}}.$$

Cochran[1] has shown that $\sigma(\partial\rho/\partial x)$ may be evaluated by determining the slope of the background resulting from the synthesis, and this has the advantage of taking account of all sources of error. In this

expression, the dominator simplifies to $-2p\rho_{peak}$, if the atom has a Gaussian distribution near the peak. Surveys of the background remote from any atom gave

$$\sigma(\partial\rho/\partial x)\approx\sigma(\partial\rho/\partial y)\approx\sigma(\partial\rho/\partial z)\approx 1.5e.\text{Å}^{-4},$$

and the value of p for each atom was determined by comparison of $\rho=\rho_0 \exp(-pr^2)$ with the ρ-values of the atom in the electron density map, giving 6.1 for sodium, 4.1 for oxygen and 6.0 for boron atoms. These values gave 0.004 Å for sodium, 0.012 Å for oxygen and 0.013 Å for boron atoms as the standard deviation, $\sigma(x)$.

The standard deviation in three dimensions, $\sigma(r)$, was estimated from $\sigma(x)$ of each atom. No error is associated with Na_1 occupying the special position (0, 0, 0). For Na_2 occupying the special position (0, y, 1/2), however, the error for its y-parameter must be considered and it is 0.004 Å same as $\sigma(x)$. The standard deviation $\sigma(r)$ for oxygen and boron atoms was estimated as 0.021 Å and 0.022 Å respectively.

Location of hydrogen atoms

As mentioned above, it was impossible to find the location of ten independent hydrogen atoms in the unit cell and to distinguish between O^{2-}, OH^- and H_2O groups only by means of the electron density distribution.

Table 3. Electrostatic valencies at oxygen atoms in borax.

Atoms	Neighbours	Electrostatic valencies	Supposed role in borax
O_1	B_1, B_1	1.50	O^{2-}
O_2	B_1, B_2	1.75	O^{2-}
O_3	B_1, B_2	1.75	O^{2-}
O_4	B_1	0.75	OH^-
O_5	B_2	1.00	OH^-
O_6	Na_1, Na_2	0.33	H_2O
O_7	Na_1, Na_2	0.33	H_2O
O_8	Na_1	0.17	H_2O
O_9	Na_2	0.17	H_2O

The consideration of the electrostatic valencies at the oxygen atoms, however, obviously shows the difference of their parts in the structure, as shown in Table 3. These distribution of electrostatic valencies can best be represented by taking O_1, O_2 and O_3 (in Table 1 & Table 3) as O^{2-}, O^4 and O^5 as OH^-, and O^6, O^7, O^8 and O^9 as H_2O.

On the other hand, among the distances between oxygen atoms where they are not coordinated to the same cation, eleven give the short distances of less than 3.1 Å and the rest all greater than 3.3 Å which must be classed as van der Waals contacts. These short distances, given in Table 4, may be regarded to suggest the places where the ten hydrogen atoms form hydrogen bonds. From the

Table 4. The distances between oxygen atoms shorter than 3.6 Å in borax, excluding those coordinated to the same cation. The distances considered to form hydrogen bonds are shown with stars.

Oxygen-oxygen	Distance (Å)
O_3—O_5	2.74*
O_1—O_8	2.75*
O_2—O_7	2.82*
O_4—O_6	2.84*
O_4—O_9	2.86*
O_5—O_6	2.86*
O_4—O_7	2.92*
O_8—O_9	2.94*
O_5—O_8	3.11*
O_3—O_9	3.12*
O_4—O_5	3.17
O_1—O_7	3.32
O_2—O_8	3.32
O_4—O_6	3.36
O_2—O_9	3.44
O_3—O_8	3.44
O_2—O_9	3.46
O_4—O_7	3.54
O_6—O_6	3.56

consideration of the tetrahedral or triangular bonds around the oxygen atoms as often observed in many other structures, ten hydrogen atoms were distributed over ten positions out of eleven as given in Table 4. The tetrahedral and triangular arrangements of bonds around the oxygen atoms in borax are shown schematically in Fig. 3, where the probable positions of hydrogen atoms are also drawn.

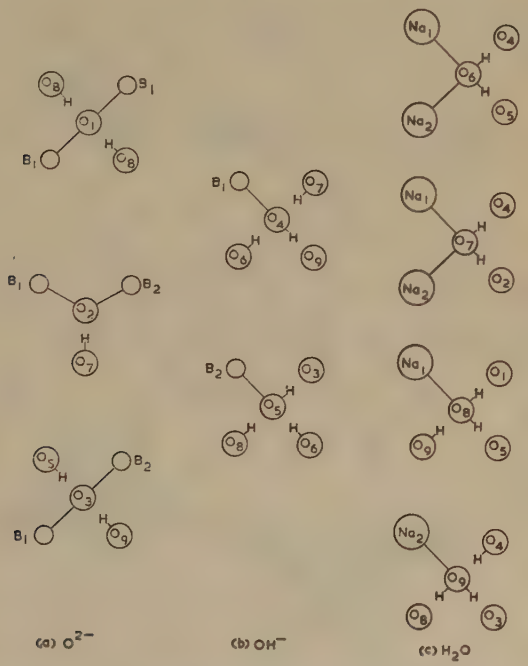

Fig. 3. The tetrahedral or triangular arrangement of bonds around the oxygen atoms in borax. The probable position of hydrogen atoms are drawn.

This result has certified the identification of atoms arrived at by the electrostatic valencies in the last paragraph.

Description of the structure

The structure of borax is projected on to (100), (010) and (001) in Fig. 4 (a), (b) and (c) respectively. In these figures, the atoms

in only half of the unit cell are shown.

It is clear from the figures that the structure of borax consists of two constituent units, that is, the chains formed by sodium atoms and water molecules, and isolated groups formed by the rest of the constituent atoms. The chains have the composition of $Na_2 \cdot 8H_2O$ and are built up with octahedra of water molecules around Na, which

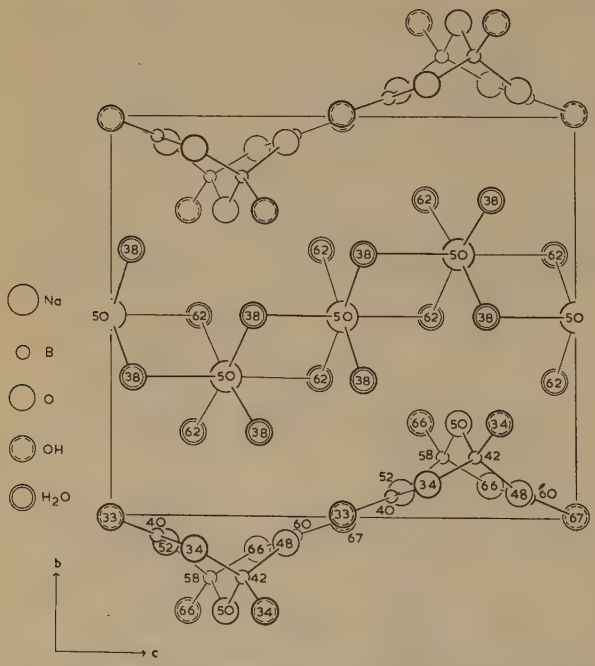

Fig. 4. The structure of borax. Numbers give the height of each atom in the cell expressed as a percentage of the a_0-, b_0- or c_0-translation.

(a) Projection on (100). Only the atoms forming a single sheet are shown.

(b) Projection on (010). Only the middle half of the unit cell is shown. Broken lines represent the hydrogen bonds holding the isolated group $B_4O_5(OH)_4$ to each other.

(c) Projection on (001). Only the lower half of the unit cell is shown.

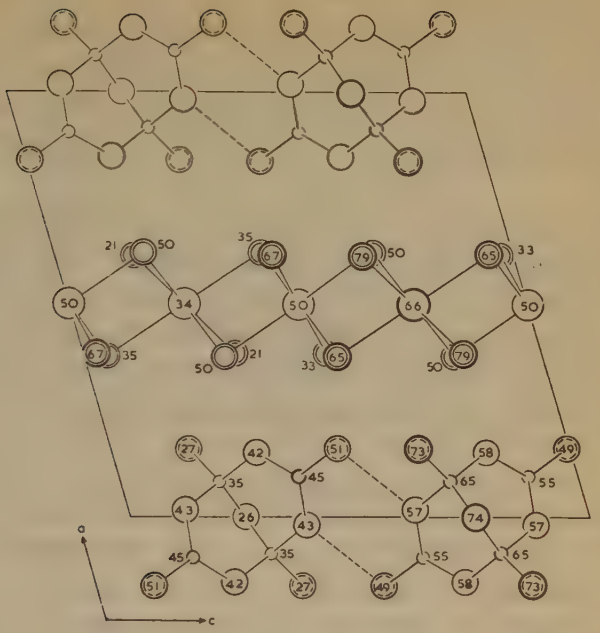

(b)

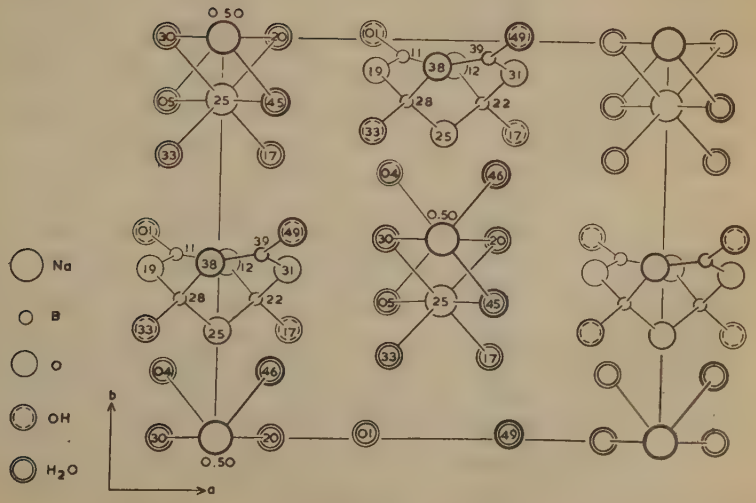

(c)

link each other by holding the H_2O–H_2O edges in common. These chains are stretched parallel to each other and to the c-axis. The isolated groups are composed of two tetrahedra formed by O^{2-} and OH^- around B_1 and two triangles formed by O^{2-} and OH^- around B_2 by sharing some of O^{2-} so as to make the composition of $B_4O_5(OH)_4$.

The isolated groups are placed in between the chains to make a sheet parallel to (100), the attraction between them being due to the hydrogen bonds. In this sheet, moreover, the isolated groups are connected with the neighbouring ones through the hydrogen bonds between O_3 and O_5 ($O_3\cdots H-O_5$: 2.74 Å), and make a chain parallel to the chains of water molecules around Na. This relation

Table 5. Interatomic distances in borax (in Å).

1. Octahedron around Na_1	
Na_1—O_6	2.40
Na_1—O_7	2.44
Na_1—O_8	2.40
O_6—O_7	3.39, 3.41
O_6—O_8	3.36, 3.40
O_7—O_8	3.38, 3.44

2. Octahedron around Na_2	
Na_2—O_6	2.45
Na_2—O_7	2.44
Na_2—O_9	2.40
O_6—O_7	3.39, 3.50
O_6—O_1	3.17, 3.68
O_7—O_9	3.16, 3.16

3. Tetrahedron around B_1	
B_1—O_1	1.47
B_1—O_2	1.46
B_1—O_3	1.54
B_1—O_4	1.46
O_1—O_2	2.42
O_1—O_3	2.44
O_1—O_4	2.40
O_2—O_3	2.43
O_2—O_4	2.42
O_3—O_4	2.40

4. Triangle around B_2	
B_2—O_2	1.36
B_2—O_3	1.32
B_2—O_5	1.40
O_2—O_3	2.38
O_2—O_5	2.34
O_3—O_5	2.34

is clearly shown in Fig. 4 (b), in which the hydrogen bonds connecting the isolated groups are given specially. Therefore, this structure is best expressed by the formula $B_4O_5(OH)_4 \cdot Na_28H_2O$. The perfect cleavage parallel to (100) may be explained from this structure, since (100) is the direction of the extention of sheets which are held together mainly by hydrogen bonds.

The interatomic distances in this structure are given in Table 5. It follows from the accuracy of this structure that Na–O distances have a standard error of 0.02 Å, B–O distances of 0.03 Å and O–O distances of 0.03 Å. The octahedron formed by water molecules around Na_1 is a regular one within the limits of error, but those around Na_2 is a little distorted. The mean values of interatomic distances Na–H_2O and H_2O–H_2O are 2.42 Å, and 3.45 Å respectively, in which the distance Na–H_2O is a little larger than the sum of the Goldschmidt radii, 2.30 Å. B_1 is coordinated by four neighbours, one OH^- and three O^{2-}, arranged at the corners of a regular tetrahedron. The mean interatomic distances B–O(OH) and O–O (OH) are 1.48 Å and 2.42 Å respectively. These tetrahedra are found in datolite[6] with the interatomic distances B–O(OH) 1.49 Å and O–O(OH) 2.43 Å. B_2 has three neighbours triangularly, one OH^- and two O^{2-}. The mean values of B–O(OH) and O–O(OH) are 1.36 Å and 2.35 Å respectively, which are comparable with the triangle $B(OH)_3$ in boric acid[13], 1.36 Å of B–OH and 2.356 Å of OH–OH.

Acknowledgement

The author wishes to express his sincere thanks to Prof. T. Ito, M. J. A. for his valuable suggestions and guidances during the course of this work, and to Dr. R. Sadanaga for his critical discussions and advice. He is also indebted to Mr. Y. Iitaka for his help in estimation of the lattice constants of borax with "Norelco" X-ray diffractometer and his valuable discussions. His thanks are also due to Prof. T. Watanabe, of the Geological Institute, University of Tokyo, and to Prof. N. Katayama and Dr. H. Minato, College

of General Education, University of Tokyo, for their help and encouragements in this work.

References

1) Cochran, W.: Acta Cryst., **4**, 81 (1951).
2) Cochran, W.: Acta Cryst., **5**, 65 (1952).
3) Cochran, W. & B. R. Penfold: Acta Cryst., **5**, 644 (1952).
4) Font Tullot, José Ma.: Estud. Geol., **7**, 13 (1947).
5) Harker, D., & J. S. Kasper: Acta Cryst., **1**, 70 (1948).
6) Ito, T. & H. Mori: Acta Cryst., **6**, 24 (1953).
7) Megaw, H. D.: Acta Cryst., **7**, 771 (1954).
8) Minder, W.: Zeit. Krist., **92**, 301 (1935).
9) Structure Reports for 1947-1948, **2**, 431.
10) Wiebenga, E. H. & D. W. Smits: Acta Cryst., **3**, 265 (1950).
11) Willson, A. J. C.: Acta Cryst., **2**, 318 (1949).
12) Zachariasen, W. H.: Acta Cryst., **5**, 68 (1952).
13) Zachariasen, W. H.: Acta Cryst., **7**, 305 (1954).

Manuscript received March 25, 1956.

Mineralogical Journal, Vol. 2, No.1, pp. 19-26, Dec., 1956

THE CRYSTAL STRUCTURE OF VONSENITE

Yoshio Takéuchi

Mineralogical Institute, University of Tokyo

Abstract

The crystal structure of vonsenite (iron-rich ludwigite) was determined by two dimensional Fourier synthesis. The unit cell has the dimensions, a_0= 9.73 Å, b_0=12.35 Å, c_0=3.05 Å. The space group is Pbam. The structure is essentially the same as the structure of ludwigite obtained by earlier study. However, the present work was based upon much more accurate intensity data, so that the results provide a knowledge of the interatomic distances in detail.

Introduction

The structure of ludwigite* as found by trial-and-error investigation[4] was believed to be essentially correct with regard to the general location of the atoms, since there was a good agreement between computed and observed intensities. Also, it has been known that the locations of magnesium and iron atoms show a good agreement with those of a synthetical compound which was later published by Bertaut[1]. Nevertheless, the accuracy of parameters of the rest of the atoms, especially that of the boron atom, being quite unknown, the refinement of the structure was undertaken using an iron rich ludwigite which is particularly named as vonsenite.

The earlier work had already shown that all atoms of ludwigite were confined to the (001) reflection planes. The refinement was, accordingly, carried out using the two dimensional Fourier method.

The chemical composition of vonsenite from Riverside, Riverside

* The refinement of the structure of ludwigite has been undertaken by Jair Carvalho da Silva, Joan R. Clark and C. L. Christ (see the program of The 36th Annual Meeting of The Mineralogical Society of America, 1955).

County, California has been reported as follows[3]: FeO 39.75%, MgO 10.71%, Fe_2O_3 34.82%, B_2O_3 14.12%, total 99.40%.

From above data, the cell formula of vonsenite is derived to be

$$8\,(Fe_{0.625}Mg_{0.375})\,O \cdot 2Fe_2O_3 \cdot 2B_2O_3.$$

The lattice constants of the orthorhombic unit cell are

$a_0=9.73_0$ Å,

$b_0=12.35_7$ Å,

and $c_0=3.05_5$ Å,

which give the specific gravity 4.24 in agreement with 4.21 as observed by Eakle[3]. The space group is Pbam.

Refinement of the structure

The refinement of the structure reported here was based upon *hk*0 reflections as recorded on equi-inclination Weissenberg photographs (Cu K_α radiation, $\lambda=1.5418$ Å). Intensities were estimated visually by the multiple film technique using intensity scale prepared from a reflection of the same crystal which was used for recording the *hk*0 reflections. The cross section of the crystal used was roughly square and small enough so that differences in absorption for different planes were not large enough to be significant. Since the crystal structure of ludwigite had been known, for the purpose of refining the structure of vonsenite, the measured F values were placed on an absolute scale by multiplying them the factor which gives the closest agreement between measured and calculated F values. The absolute scale of the structure factors thus obtained were slightly improved when the structure was considerably refined.

The coordinates of atoms, except boron atom, resulting from the trial-and-error structure determination of ludwigite were used as a starting point of the refinement. The phases determined by these coordinates were applied to the amplitude F_{hk0}. Thus, the first electron density projection $\rho\,(xy)$ was computed on X-RAC, with

the kind permission of Professor Ray Pepinsky. In this electron density projection, all atoms were quite well resolved. Taking the center of these peaks for new locations of atoms, new phases of F_{hk0} were determined.

By subtracting the contribution of iron atoms, F_{iron}, from observed

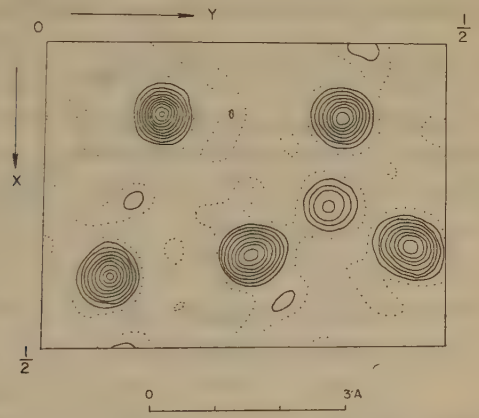

Fig. 1. The final difference synthesis $\Delta'\rho(xy)$. Broken line indicates zero contour.

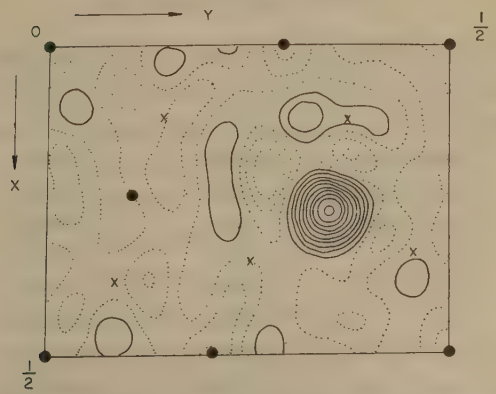

Fig. 2. The final difference synthesis $\Delta\rho(xy)$. Zero and negative contours are broken. The locations of iron and oxygen atoms are marked by solid circles and crosses respectively.

F values, the difference synthesis $\Delta'\rho(xy)$, using as Fourier coefficients $(F_{obs}-F_{iron})_{hk0}$, was successively employed for the further refinement of the structure. The last stage, since the atoms are substantially in their positions, the difference synthesis $\Delta\rho(xy)=\rho_c(xy)-\rho_o(xy)$ was computed. The location of boron atom was established in the final difference electron density projection $\Delta\rho(xy)$ (Fig. 2).

To the final structure, the residual factor, $R=\frac{||F_o|-|F_c||}{|F_o|}$, was reduced to less than 9% for the $hk0$ reflections. The final difference

Table 1. Coordinates of atoms.

Atom	x/a_0	y/b_0	z/c_0	No. of atoms in the cell
O_1	0.160	−0.045	0	4
O_2	0.114	0.146	1/2	4
O_3	0.125	0.375	0	4
O_4	0.384	0.085	1/2	4
O_5	0.350	0.260	0	4
B	0.271	0.355	0	4
$Fe^{++}(Mg)_1$	0	0	1/2	2
$Fe^{++}(Mg)_2$	1/2	0	0	2
$Fe^{++}(Mg)_3$	−0.001	0.277	1/2	4
Fe^{+++}	0.247	0.114	0	4

Table 2. Termination error of Fourier series.

Atom	x (Å)	y (Å)
$Fe^{++}(Mg)_1$	0.000	0.000
$Fe^{++}(Mg)_2$	0.000	0.000
$Fe^{++}(Mg)_3$	0.000	0.008
Fe^{+++}	0.004	0.010
O_1	0.016	0.022
O_2	0.008	0.012
O_3	0.014	0.016
O_4	0.018	0.020
O_5	0.007	0.010
B	0.010	0.035

synthesis $\Delta'\rho(xy)$ is shown in Fig. 1. The coordinates of atoms found in the final structure of vonsenite are given in Table 1.

Accuracy of the coordinates

The termination error of the Fourier series was evaluated in the usual way by summing a Fourier series using the calculated structure factors as the coefficients. The error in the atomic coordinates in the ($hk0$) projection as given by $\Delta x_j = |x_{j,\,obs} - x_{j,\,calc}|$ and $\Delta y_j = |y_{j,\,obs} - y_{j,\,calc}|$ are listed in Table 2. The coordinates of iron atoms are very well established in the Fourier projection. There was very little drift in the coordinates of these atoms during refinement. For these reasons, it is unlikely that error of coordinates for iron atoms exceeds more than ± 0.001 as decimal fraction of the axis.

For the estimation of probable error of oxygen and boron atoms, Cruickshank's method[2] was also applied. The standard deviation $\sigma(r)$ which is taken as $[\sigma(x)^2+\sigma(y)^2]^{\frac{1}{2}}$ was evaluated for oxygen and boron atoms as follows:

for oxygen atoms.....1.9×10^{-2} Å,
for boron atoms .....3.0×10^{-2} Å.

Discussion of the structure

A packing drawing of the structure of vonsenite as illustrated in Fig. 3 is essentially the same as the structure of ludwigite obtained by the previous work except considerable shifting of some of the oxygen atoms. Although iron content of vonsenite is much higher than that of the crystal used in the earlier investigation, the shifting of oxygen atom is obviously due to the accuracy of the work. In this sense, the atomic positions found in vonsenite will improve the interatomic distances of ludwigite as well.

Iron atoms are surrounded by six oxygen atoms octahedrally. The interatomic distances are shown in Fig. 4 and Fig. 5. The mean value of Fe^{++}—O distances is 2.16 Å and 2.05 Å for Fe^{+++}—O distances. The boron triangle is slightly distorted, O'_1—O_3 edge being

Table 3. Comparison of observed and calculated F-values.

$hk0$	F_0	F_c	$hk0$	F_0	F_c	$hk0$	F_0	F_c
110	16	−21	470	9	−13	810	10	13
120	65	−70	480	75	78	820	0	2
130	26	27	490	17	−13	830	10	8
140	15	−16	4.10.0	72	74	840	0	1
150	15	−10	4.11.0	0	4	850	0	3
160	63	67	4.12.0	0	0	860	0	0
170	40	37	4.13.0	0	0	870	10	−13
180	45	39	4.14.0	14	11	880	70	68
190	53	−51				890	20	18
1.10.0	17	−16	510	13	16	8.10.0	44	45
1.11.0	17	18	520	50	−48	8.11.0	13	13
1.12.0	27	−28	530	0	−2			
1.13.0	24	−19	540	16	−16	910	0	0
1.14.0	16	19	550	41	−41	920	30	−33
			560	26	24	930	10	−1
200	38	41	570	25	28	640	13	−11
210	0	1	580	24	24	950	40	−45
220	0	0	590	38	−31	960	31	29
230	0	−8	5.10.0	40	−38	970	50	45
240	154	160	5.11.0	35	30	980	19	15
250	72	70	5.12.0	30	−30	990	13	−8
260	52	51	5.13.0	36	−37	9.10.0	12	−12
270	0	0	5.14.0	16	18			
280	11	9				10.0.0	18	23
290	21	−19	600	25	54	10.1.0	16	−13
2.10.0	26	33	610	0	−6	10.2.0	0	0
2.11.0	15	−16	620	0	1	10.3.0	10	−15
2.12.0	47	40	630	0	3	10.4.0	57	58
2.13.0	15	13	640	153	152	10.5.0	12	17
2.14.0	72	68	650	31	−33	10.6.0	32	33
			660	27	27	10.7.0	19	20
310	26	−26	670	10	7	10.8.0	6	7
320	55	−52	680	10	−9	10.9.0	0	−1
330	14	22	690	19	18			
340	18	18	6.10.0	0	1	11.1.0	17	−15
350	45	−49	6.11.0	0	0	11.2.0	18	18
360	44	−47	6.12.0	34	31	11.3.0	21	21
370	40	−37	6.13.0	14	−14	11.4.0	0	2
380	34	−32				11.5.0	0	0
390	49	−45	710	12	−13	11.6.0	30	−28
3.10.0	43	42	720	50	53			
3.11.0	59	54	730	30	32	12.1.0	5	−6
3.12.0	36	30	740	18	20	12.2.0	5	4
3.13.0	24	−20	750	0	4			
3.14.0	17	−15	760	22	−22	020	18	17
			770	10	17	040	6	4
400	71	73	780	28	−23	060	5	−10
410	9	−9	790	50	−50	080	112	113
420	12	16	7.10.0	27	27	0.10.0	49	51
430	13	14	7.11.0	20	19	0.12.0	0	−8
440	40	40	7.12.0	20	20	0.14.0	31	25
450	13	−13						
460	11	11	800	135	143			

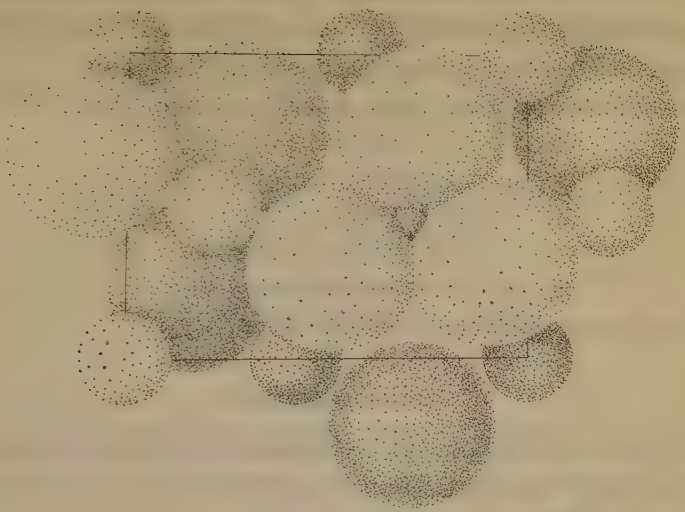

Fig. 3. A packing drawing of the structure of vonsenite. Quarter of cell is outlined. Atomic positions correspond to those indicated in Fig. 2.

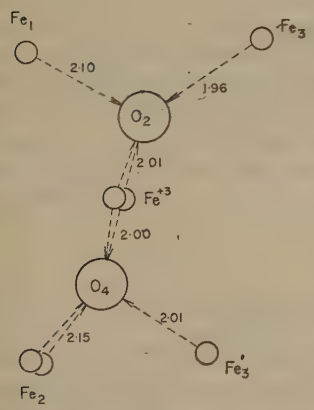

Fig. 4.

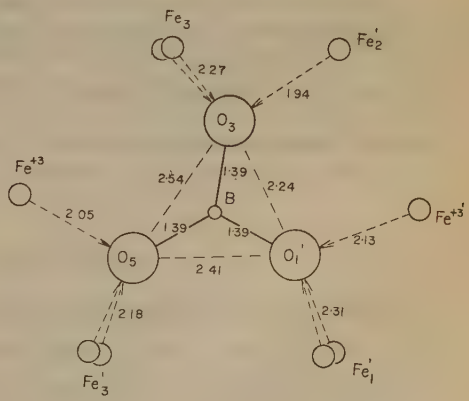

Fig. 5.

Fig. 4. Configuration of iron atoms about oxygen atoms. Interatomic distances are shown.

Fig. 5. Configuration of iron atoms about BO_3 group. Interatomic distances are shown.

10% shorter than the other edges. This might be due to closer approach of Fe^{++}_2 and Fe^{+++} atoms to the boron atom. The bond distances of the boron triangle is shown in Fig. 5.

The electrostatic bonds terminating to oxygen atoms are:

O_2.....1+2×2/6+3/6=2.1/6,
O_2.....2/6+2/6+2×3/6=1.2/3,
O_3.....2×2/6+2/6+1=2,
O_4.....2×3/6+2×2/6+2/6=2,
O_5.....2×1/6+3/6+1=2.1/6.

The conformity of Pauling's rule is satisfactory.

Acknowledgements

This work was done in the Department of Physics of the Pennsylvania State University. I wish to thank Professor Ray Pepinsky for the facilities and kind advise.

References

1) Bertaut, E.F.: Acta Cryst., **3**, 473 (1950).
2) Cruickshank, D.W.: Acta Cryst., **2**, 154 (1949).
3) Eakle: Am. Min., **5**, 141 (1920).
4) Takéuchi, Y., T. Ito and T. Watanabe: Acta Cryst., **3**, 98 (1950).

Manuscript received July 30, 1956.

Mineralogical Journal, Vol. 2, No. 1, pp. 27-38, Dec., 1956

CHEMICAL STUDIES OF LITHIUM MICAS FROM THE PEGMATITE OF MINAGI, OKAYAMA PREFECTURE

Yasuo Ukai, Shin'ichi Nishimura and Yoshikazu Hashimoto

Geological and Mineralogical Institute, Faculty of Science, University of Kyoto

Abstract

The chemical compositions of lithium micas in a pegmatite at Minagi, Okayama Prefecture, were studied. This pegmatite consists of five zones; (1) border zone, (2) biotite zone, (3) muscovite zone, (4) zinnwaldite zone and (4) lepidolite zone, arranged inwards successively. Each zone is characterized by their mineral assemblage, especially by the varieties of mica comprised in it.

It appears that iron and magnesium fit better into the mica structure than does lithium, and in the earlier stage the greater part of these elements are removed from the pegmatite solution forming biotite crystals. In the last stage of the cooling history of this pegmatite, the residual solution in which lithium had been gradually concentrated replaced the pre-existing feldspar, producing the lithium micas and secondary greenish violet hydrous alumina minerals. In the later stage, hydrothermal replacement is very remarkable and this is one of the distinctive characteristics of the lithium mica bearing pegmatite.

Introduction

From the view point of crystallochemistry, lithium differs in behavior so pronouncedly from other alkali metals that it often forms characteristic minerals in pegmatite, but it never enters the feldspar structures. The polymorphism of muscovite-lepidolite series has been investigated in detail by Levinson[10], and Hendricks and Jefferson[6], but many problems of biotite-zinnwaldite-lepidolite series which is common in pegmatite have been overlooked. In this paper the present writers will report the results of chemical studies on

lithium micas from a pegmatite at Minagi, Okayama Prefecture, taking into consideration the cation substitution in octahedral layer of mica structure, and also discuss their distinguished features in the course of crystallization of the pegmatite.

Locality and general geology (Fig. 1)

The pegmatite under consideration[16] is located at about seven kilometers north of the Minagi* station on the Hakubi railway line.

This region is composed of Palaeozoic system and later igneous rocks i. e. quartz-porphyry, biotite-granite, biotite-hornblende-granite, diorite and acidic dykes.

The Palaeozoic system consists mainly of black shale, clay-slate and schalstein. Black shale and clay-slate are distributed in the southern part of the district with the general strike N. 80° E. and dipping 75° N..

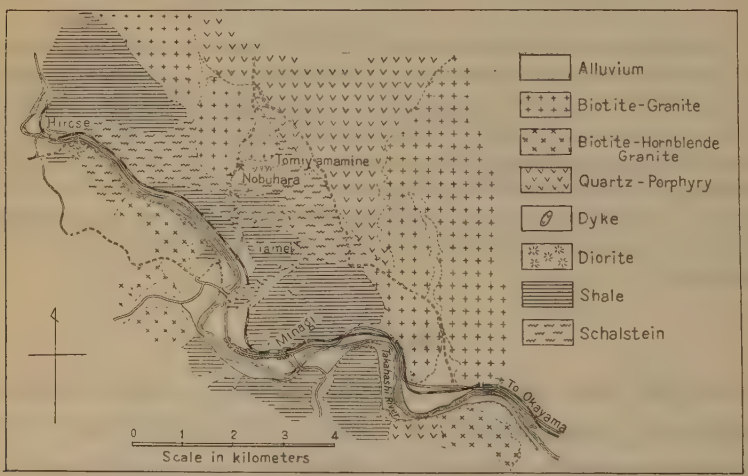

Fig. 1. Geological map of the Minagi district.

Zonal arrangement in the Minagi pegmatite

In this district many pegmatites have been found in the Palaeozoic

* 美袋

system close to the biotite-granite. The pegmatite now under consideration, the most representative in this district, crops out in a area of metamorphosed schalstein which contains a large amount of green alkali-hornblendes due to the contact effects of the biotite-granite.

In this pegmatite several zones[3] are distinguished according to mineral associations, especially with respects to feldspar and lithium mica. They are enumerated inwards respectively as border zone, biotite zone, muscovite zone, zinnwaldite zone and lepidolite zone.

The border zone is narrow and relatively fine-grained. It comprises, besides the essential members such as oligoclase, albite and quartz, a variety of contact minerals such as green alkali hornblende, garnet and epidote.

The biotite zone commonly contains fine flakes of biotites, besides oligoclase, microcline and quartz. The thickness of this zone varies considerably. The boundary toward the border zone is generally indistinct.

Zircon is contained as an accessory mineral, and when enclosed by biotite, it is surrounded by intense pleochroic halo. In this zone, the colour of biotite from periphery is black, while it becomes dark brown to grey inwardly.

The muscovite zone is characterized by the large amount of muscovite flakes. The other common minerals in this zone are microcline and subordinate zinnwaldite. The colour of muscovite is usually grey in the part adjacent to the biotite zone, while it becomes dark brown towards the inner zone, and again changes gradually to pale brown in the zinnwaldite zone.

The variations in thickness of the pegmatite are mostly due to the irregularity in developement of these zones. Where the pegmatite pinches the muscovite zone either disappears entirely or mingles with the biotite zone to form a mixed one.

The zinnwaldite zone is always accompanied by zinnwaldite as a characteristic mineral. The muscovite and the zinnwaldite zones

Table 1. Mineral association of each zone.

Border zone	Biotite zone	Muscovite zone	Zinnwaldite zone	Lepidolite zone
Oligoclase	Microcline	Microcline	Oligoclase	Plagioclase
Quartz	Oligoclase	Quartz	Albite	Amazonstone
Albite	Quartz	Muscovite*	Microcline	Rosy quartz
Epidote	Biotite*	Zircon	Zinnwaldite*	Lepidolite*
Green hornblende	Green hornblende	Albite	Rosy quartz	Green mica
Garnet	Zircon		Muscovite	Greenish violet hydrous alumina
	Sphene		Lepidolite	

* Representative mica in each zone.

generally shade into each other, some muscovite being disseminated in the latter zone as well. This zone also changes gradually into the lepidolite zone. The most common minerals in this zone are zinnwaldite, albite, oligoclase, quartz and small quantity of muscovite. The quartz in this zone is chiefly found as rosy quartz, and microcline is rarely found.

The lepidolite zone, the innermost part of pegmatite, contains

Fig. 2. Schematic diagram showing the zonal arrangement in the Minagi pegmatite.

Le: lepidolite, M: muscovite, B: biotite, A: amazonstone, Z: zinnwaldite, Q: quartz, G: garnet.
I: border zone, II: biotite zone, III: muscovite zone, IV: zinnwaldite zone, V: lepidolite zone.

lepidolite, amazonstone, rosy quartz and a greenish violet, massive, hydrous alumina mineral. At times, green mica is found surrounded by lepidolite. This zone is characterized by the replacement of the pre-existing mineral by the residual hydrothermal solution.

The general aspects of the zonal arrangement in the Minagi pegmatite is illustrated schematically in Fig. 2, and the mineral association in each zone is summarized in Table 1.

Chemical composition of mica and feldspar in each zone

The micas and feldspars in each zone were analysed chemically. The results are tabulated in Tables 2 and 3 and plotted in three components diagram as Figs. 3 and 4.

Table 2. Chemical composition of averaged material of feldspars in each zone.

	(a) Biotite zone	(b) Muscovite zone	(c) Zinnwaldite zone	(d) Lepidolite zone
SiO_2	65.25%	65.61%	68.16%	67.05%
Al_2O_3	20.56	19.55	20.56	20.70
CaO	0.76	0.20	0.06	1.14
MgO	0.14	0.47	0.18	1.03
K_2O	6.98	7.97	0.51	0.10
Na_2O	6.12	5.22	10.20	9.60
$H_2O(+)$	0.10	0.18	0.12	n.d.
Total	99.91%	99.20%	99.79%	99.62%

As obvious in Fig. 3 or Table 2, the average compositions of feldspars of the outer two zones are rich in potassium, while those of the inner two zones are rich in sodium. Calcium content is increased a little in the innermost zone.

The chemical composition of mica varies towards the inner zone as follows: (a) Li, F and K increase, (b) Ca, Mg and ferrous iron decrease, (c) Ti content is almont constant, and (d) Mn, Rb and Cs once increase and then decrease.

Table 3. Chemical composition of mica.

	(1) Biotite from biotite zone	(2) Muscovite from muscov. zone	(3) Zinnwaldite from zinnw. zone	(4) Lepidolite from lepid. zone	(5) Lepid. from Minagi	(6) Zinnw. from Minagi	(7) Lepid. from Okirai* [13]	(8) Lepid. from Nagatare** [13]	(9) Zinnw. from Naegi*** [14]
SiO_2	37.71%	45.80%	38.78%	51.37%	50.83%	39.03%	53.61%	50.23%	41.04%
Al_2O_3	15.30	21.21	8.84	21.61	23.70	19.57	16.32	23.56	19.35
Fe_2O_3	2.91	2.78	19.61	——	——	1.40	——	——	2.93
FeO	24.55	6.18	5.00	0.90	1.24	4.58	1.35	0.39	12.99
TiO_2	0.54	tr.	0.17	tr.	tr.	tr.	tr.	tr.	0.10
MnO	1.07	4.80	2.91	2.05	0.97	3.86	0.73	0.19	2.66
MgO	1.65	0.57	0.54	0.49	0.46	4.75	0.46	0.03	0.42
Li_2O	1.55	2.59	3.30	4.99	5.51	2.92	6.55	5.83	3.20
CaO	1.50	0.72	0.94	0.68	0.24	8.13	0.58	0.91	0.16
Na_2O	0.64	1.29	1.06	0.47	1.06	0.46	0.94	1.21	0.95
K_2O	6.29	8.89	10.34	11.99	9.88	7.91	10.90	10.88	10.78
$(Rb, Cs)_2O$	0.58	2.04	3.29	0.76	1.64	1.00	1.98	2.00	0.98
$H_2O(-)$	2.20	0.38	0.54	0.30	0.12	1.06	0.56	0.26	0.42
$H_2O(+)$	0.91	0.44	1.30	0.70	0.90	2.49	0.68	1.30	0.39
F	5.00	5.78	6.40	6.72	6.96	5.19	7.90	6.21	7.67
$O=F_2$	−2.11	−2.43	−2.69	−2.83	−2.93	−2.19	−3.33	−2.61	−3.23
Total	100.29%	101.04%	100.31%	100.20%	100.58%	100.16%	99.23%	100.39%	100.81%

* 越喜来, ** 長垂, ***苗木.

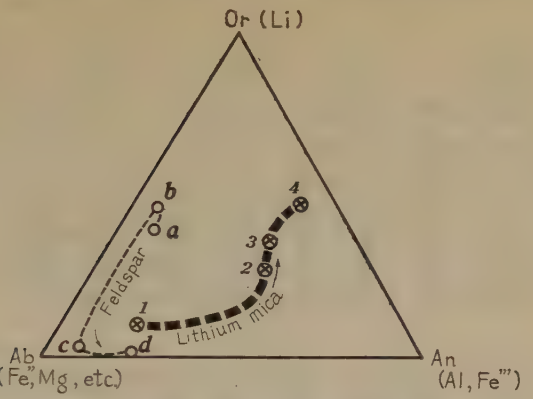

Fig. 3. Three components diagram of feldspar and lithium mica. a~d refer to those in Table 2, and 1~4 refer to those in Table 3.

Relationship between the crystal stucture and the chemical composition of lithium micas

R. E. Stevens[15] presented seventeen analyses of lepidolite and suggested five ideal formulae, polylithionite to lithium muscovite. These samples were also structurally investigated by Hendricks and Jefferson[6], and polymorphic relation in reference to Li_2O content was restudied. Recently A. Levinson[10] demonstrated the existence of a complete polymorphic series between muscovite and lepidolite. Thus the muscovite-lepidolite series have been precisely investigated from chemical and structural standpoints, while the study on micas of biotite-zinnwaldite-lepidolite series which often occur side by side in pegmatite has not been done.

The ideal formulae[2)4)] of mica unit cell are represented as follows:

	muscovite	$K_4Al_8Al_4Si_{12}O_{40}(OH, F)_8$,
	biotite	$K_4(Fe, Mg, Mn)_{12}Al_4Si_{12}O_{40}(OH, F)_8$,
	zinnwaldite	$K_4Li_4(Fe, Mn)_4Al_4Al_4Si_{12}O_{40}(OH, F)_8$,
	polylithionite	$K_4Li_8Al_4Si_{16}O_{40}(OH, F)_8$,
and	lithium muscovite	$K_4Li_6Al_6Al_4Si_{12}O_{40}(OH, F)_8$.

The formulae of various micas collected from the Minagi pegmatite

Table 4. Chemical formulae of various lithium micas.

No. in Table 3.	Chemical formula	Classification
(1)	$K_{3.54}\ Li_{1.96}\ R''_{7.53}\ Al_{2.35}\ Al_{4.14}\ Si_{11.86}\ O_{40.58}\ (OH, F)_{6.88}$ $= K_4Li_2R''_8\ Al_2Al_4Si_{12}O_{41}(OH, F)_7$	Lithium bearing biotite
(2)	$K_{4.53}\ Li_{2.97}\ R''_{2.87}\ Al_{4.76}\ Al_{2.96}\ Si_{13.04}\ O_{41.36}\ (OHF,)_{6.03}$ $= K_5Li_3R''_3\ Al_5Al_3Si_{13}O_{41}(OH, F)_6$	Zinnwaldite member
(3)	$K_{5.96}\ Li_{4.30}\ R''_{2.42}\ Al_{4.78}\ Al_{3.38}\ Si_{12.60}\ O_{40.46}\ (OH, F)_{9.36}$ $= K_6Li_4R''_2\ Al_5Al_3Si_{13}O_{40}(OH, F)_9$	Zinnwaldite member
(4)	$K_{4.75}\ Li_{5.47}\ R''_{0.89}\ Al_{4.93}\ Al_{2.01}\ Si_{13.99}\ O_{40.95}\ (OH, F)_{7.06}$ $= K_5Li_6R''_1\ Al_5Al_2Si_{14}O_{41}(OH, F)_7$	Lepidolite C-type*
(5)	$K_{4.27}\ Li_{5.92}\ R''_{0.69}\ Al_{5.04}\ Al_{2.42}\ Si_{13.58}\ O_{40.43}\ (OH, F)_{7.48}$ $= K_4Li_6Al_5Al_2Si_{14}O_{40}(OH, F)_8$	Lepidolite C-type*
(6)	$K_{6.37}\ Li_{3.67}\ R''_{4.44}\ Al_{3.75}\ Al_{3.79}\ Si_{12.21}\ O_{41.39}\ (OH, F)_{10.32}$ $= K_6Li_4R''_4\ Al_4Al_4Si_{12}O_{41}(OH, F)_{10}$	Zinnwaldite
(7)	$K_{4.87}\ Li_{7.29}\ R''_{0.68}\ Al_{4.18}\ Al_{1.15}\ Si_{14.85}\ O_{40.43}\ (OH, F)_{8.18}$ $= K_5Li_7R''_1\ Al_4Al_1Si_{15}O_{41}(OH, F)_8$	Lepidolite B-type*
(8)	$K_{5.19}\ Li_{6.38}\ R''_{0.15}\ Al_{5.23}\ Al_{2.33}\ Si_{13.67}\ O_{40.80}\ (OH, F)_{7.70}$ $= K_5Li_6Al_5Al_2Si_{14}O_{41}(OH, F)_8$	Lepidolite C-type*
(9)	$K_{4.92}\ Li_{3.86}\ R''_{4.13}\ Al_{3.35}\ Al_{3.68}\ Si_{12.32}\ O_{40.46}\ (OH, F)_{8.06}$ $= K_5Li_4R''_4\ Al_4Al_4Si_{12}O_{40}(OH, F)_8$	Zinnwaldite

* After Stevens.

and other localities in Japan were calculated from the chemical compositions as tabulated in Table 4.

As have been well investigated[1)6)7)10)11)] the unit cell of mica has four silicon layers, four positions for large cations populated by K, Na, Rb, Cs and Ca, eight to twelve octahedral positions occupied by Al, Mg, Mn, Fe″, Fe‴, Ti and Li, sixteen tetrahedral positions for Si and Al, forty oxygen atoms and eight hydroxyl radicals or fluorines. Therefore, the total number of atoms in the unit cell varies from seventy six to eighty counting the hydroxyl radical (OH) as one atom.

The chemical formulae derived from the analyzed data of lithium bearing micas are generally conformable to the above mentioned relations. In detail, however, some deviations from the ideal formula are frequently met with in the number of large cation, oxygen atom and hydroxyl radical or fluorine atom. The writers therefore have classified the specimens conveniently as Table 4 referring to R.E. Stevens' classifications of lepidolite.

The manner of substitution of cations in the octahedral group is complicated, and is concerned with the variety of mica. To represent the mutual relationship of substitution, a three components diagram was devised (Fig. 4), in which for comparison chemical data of lithium bearing mica given by previous investigators[4)5)] are plotted.

Almost all micas are in the area of quadrilateral BMPQ, in which the following established stipulations will be satisfied. The number of positions for the octahedral cation vary from 8 to 12 and the equivalents of octahedral cation vary from 20 to 24 according to the degree of substitution of Si by Al in tetrahedral group.

The emphasis lies in the fact that the micas are not distributed homogeneously over the area but concentrated in several separate domains, namely biotite-, muscovite-, zinnwaldite-, lepidolite-, R- and S- region. This fact suggests, that the micas in these regions are rather stable in their crystal structures. In the tetrahedral group, $Al_4Si_{12}O_{40}$ and $Al_3Si_{13}O_{40}$ types are most common for biotite, muscovite

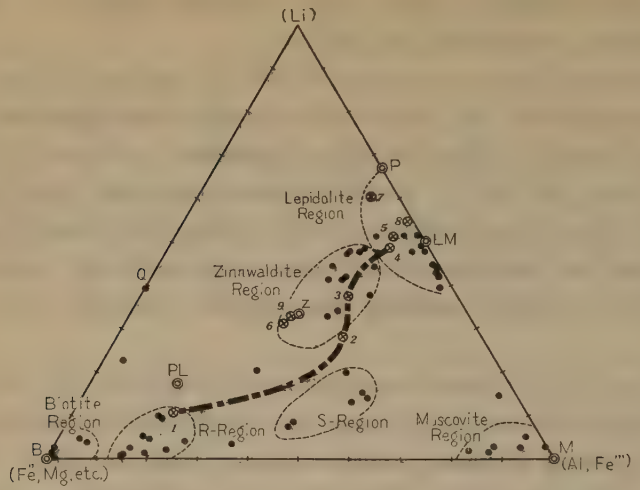

Fig. 4. Three components diagram of octahedral substitution.
1~9 refer to those in Table 3.
B: biotite, M: muscovite, Z: zinnwaldite,
LM: lithium muscovite, P: polylithionite,
PL: protolithionite, Q: point representing
octahedral cation 12, octahedral equivalent 24.

and zinnwaldite regions while $Al_2Si_{14}O_{40}$ and $Al_1Si_{15}O_{40}$ types for lepidolite region. The octahedral equivalent, accordingly, is 23~24 in the former case and 21~22 in the latter case.

Crystallization of lithium micas in the Minagi pegmatite

In general, the factors controlling the amount of elements in respective minerals are so complicated that we can not visualize the scheme of chemical behaviour in the course of crystallization of pegmatite. For instance, the variation in chemical composition of mica is not always parallel to that of feldspar which varies its composition sodic to potassic and again to sodic. From the view point of crystal chemistry, nevertheless, the present writers tried some consideration of the crystallization of lithium micas in this pegmatite.

Lithium differs very pronouncedly from the other alkali metals in its reluctance to enter the feldspar structures. The oligoclase or sodium microcline formed during the primary pegmatite stage is usually devoid of lithium and some portion of this element often replaces the divalent cation in the octahedral group of ferromagnesian mica as was demonstrated in the previous section. As will be infered from Fig. 4, however, lithium seems to be limited in amount in ferromagnesian mica of the earlier crystallization stage and concentrated gradually in the residual solution.

On the other hand, iron and magnesium appear to fit better into the mica structure than does lithium, and in the earlier stage most of these elments were removed from the pegmatite solution. As the net results, the residual solution concentrated with lithium replaced the pre-existing feldspar, producing the lithium micas proper.

Hydrothermal replacement, which is one of the characteristics of lithium mica bearing pegmatites[9)12)13)], is also very remarkable in the Minagi pegmatite, and in its inner zone perthitic microcline always shows patch perthitic structure accompanied by numerous greenish violet hydrous alumina minerals.

Acknowledgement

The writers wish to express their sincere thanks to Professor T. Ito and Emeritus Professor S. Tsuboi for their helpful suggestions and encouragements and to Assistant Professor R. Kiriyama for his valuable help and advice in carrying out the X-ray studies. A part of this work has been performed by the Scientific Grant of the Ministry of Education of the Japanese Government.

References

1) Bragg, W. L.: Atomic Structure of Minerals, 203 (1937).
2) Bragg, W. L.: Atomic Structure of Minerals, 215 (1937).
3) Camerson, E. N., et al.: Econ. Geol., Monograph 2 (1949).
4) Dana: The System of Mineralogy, 611 (1914).
5) Doelter, C.: Handbuch der Mineralogie, Band II (1917).

6) Hendricks, S. B. and M. F. Jefferson: Am. Miner., **24**, 729 (1939).
7) Jackson, W. W. and J. West: Zeit. Kryst., **76**, 211 (1930); **85**, 160 (1933).
8) Joklik, G. F.; Econ. Geol., **50**, 625 (1955).
9) Lacroix, A.: Mineralogie de Madagascar, vol. 2, 355 (1923).
10) Levinson, A.: Am. Miner., **38**, 88 (1953).
11) Pauling, L.: Proc. Nat. Acad., **16**, 123 (1930).
12) Schaller, W. T.: Am. Jour. Sci., **10**, 267 (1925).
13) Shibata, S.: Jour. Geol. Soc. Tokyo, **41**, 582 (1934). (in Japanese)
14) Shibata, S.: Jour. Geol. Soc. Tokyo, **46**, 69 (1939). (in Japanese)
15) Stevens, R. E.: Am. Miner., **23**, 607 (1938).
16) Ukai, Y. and K. Kondo: Mineralogy and Geology, Ser. **13**, 22 (1949). (in Japanese)

Manuscript received August 30, 1956

Mineralogical Journal, Vol. 2, No. 1, pp. 39-47, Dec., 1956

DEPENDENCE OF THE OPTICAL ABSORPTION ON THE CRYSTALLOGRAPHIC ORIENTATION IN HEIKOLITE*

Tokugoro Shoda

Institute of Mineralogy, University of Tokyo

Abstract

It is concluded that the principal axes of absorption ellipsoid of heikolite are as follows: X nearly $\perp$ (100), Y // [010] and Z nearly // [001]. The orientations of X and Z do not coincide with the principal axes of the indicatrix.

Introduction

In his previous paper,[2] the present writer gave an account on the study of the anomalous optical phenomena shown by heikolite, a variety of alkali amphibole, of which the (010) section does not extinguish between crossed nicols even with the monochromatic light. The writer described especially the variation of the intensity of the transmitted light on the section measured by a photometer with photomultiplier.[1] He also noted the difference between the light intensity curves thus obtained and those for aegirine which is pleochroic but shows complete extinction.

The present work was undertaken in order to study, mainly, the variation of the absorption with the orientation in the heikolite crystal.

Experimental

Four sections of heikolite were prepared for measurements with following orientations:

---

* Read at the meeting of the Mineralogical Society of Japan on October 23, 1955.

(1) $\begin{cases} \rho \fallingdotseq 90° \\ \varphi \fallingdotseq 90° \end{cases}$, (2) $\rho \fallingdotseq 0°$, (3) $\begin{cases} \rho \fallingdotseq 47° \\ \varphi \fallingdotseq 90° \end{cases}$ and (4) $\begin{cases} \rho \fallingdotseq 90° \\ \varphi \fallingdotseq 50° \end{cases}$,

where ρ and φ refer to those designated by V. Goldschmidt.

For measuring the thickness of a section of strongly pleochroic mineral, it is desirable to make a preparate which contains both the mineral under investigation and a standard transparent mineral of known birefringence. As a standard, a section parallel to the optic axis of quartz was used. This was ground together with the section (1), parallel to (100) of heikolite, to the thickness $d=$ 0.030 mm. for the first observation, then ground again to $d=0.024$ mm. for the second, and finally to $d=0.010$ mm. for the third observation. In order to determine the thickness of the samples, the retardation in the quartz section was measured by means of the Soleil- Babinet compensator.

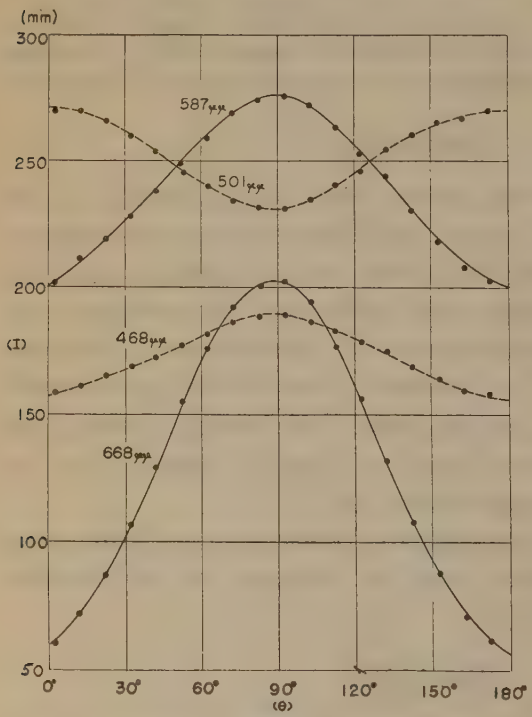

Fig. 1. Intensity variations for the (100) section of heikolite with the polarizer only. ($d=0.024$ mm.)
I: Scale readings in mm. on the apparatus.
θ: Rotation angle of the microscope stage.

The sections used in this experiments were coverd with black paper with a small hole of about 1 mm. in diameter in order to avoid the effect of the light from outside of the mineral.

The measurements were made by the polarizing microscope

with or without the universal stage. As previously reported, the intensity of light transmitted through the microscope was measured by a photometer.[1)]

Measurements on (100) section

The intensity curves obtained by the measurements with the polarizer only for the section with d=0.024 mm. are shown in Fig. 1, where the scale of intensity I is arbitrary, and θ denotes the angle between the cleavage trace and the vibration direction of polarizer.

It will be seen that for all wavelengths, the curves are symmetrical with respect to the cleavage trace. However, the direction of cleavage trace indicates the position of the maximum intensity (minimum absorption) for λ=668 mμ., λ=587 mμ. or λ=487 mμ., while it corresponds to that of the minimum for λ=501 mμ., Therefore, for the lights of certain two definite wavelengths, both the waves vibrating perpendicular or parallel to the cleavage trace are equally absorbed. These wavelengths were determined as λ=550 mμ., λ=487 mμ.. From the results of the measurements made for the (100) section with different thickness, it

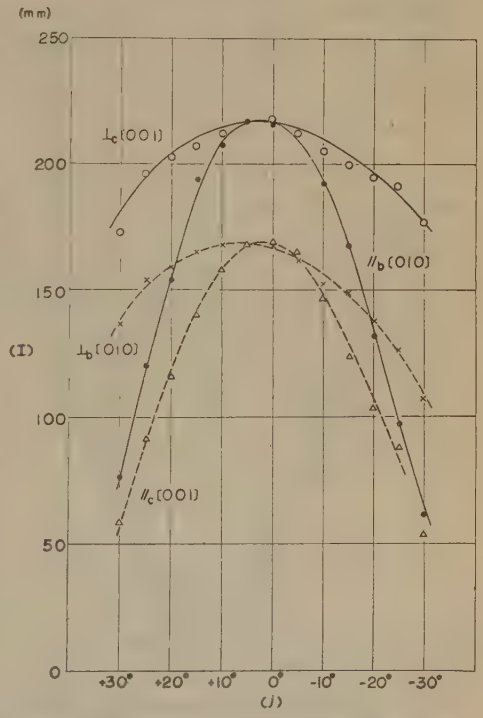

Fig. 2. Dependence of the intensity variations on direction for the (100) section of heikolite observed with universal stage. (λ=587 mμ, d=0.010 mm.)
I: Scale readings in mm. on the aparatus.
j: Rotation angle about the horizontal axis of universal stage.

was found that there was no appreciable change of the values of these wavelengths.

Rotating the section about [010] or [001] using the horizontal axis of the universal stage, and measuring the intensity in various directions, we obtained the curves showing the dependence of the intensity on direction. The results for λ=587 mμ. are shown in Fig. 2. The curves are nearly symmetrical with respect to the zero position for all wave lengths. There are two directions in which the two waves, one vibrating at right angle to the other, show the equal absorption. However, the plane including such two axes of equal absorption is parallel to the plane of (010) for λ=668 mμ., λ=587 mμ. or λ=468 mμ., whereas it is perpendicular to the plane for λ=501 mμ.. Therefore, as far as the absorption is concerned, this mineral may probably be uniaxial for the light with λ=550 mμ. or λ=487 mμ..

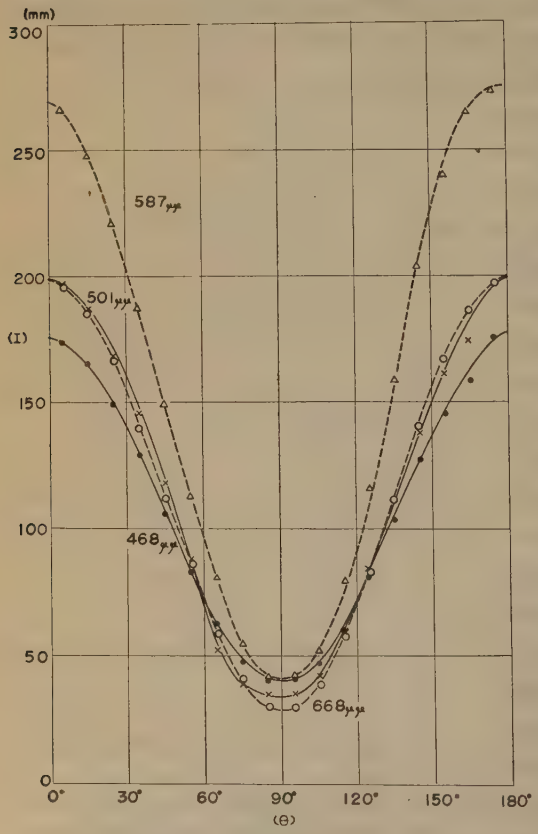

Fig. 3. Intensity variations for the section nearly perpendicular to c-axis with the polarizer only.
I: Scale readings on the apparatus.
θ: Rotation angle of the microscope stage.

The intensity curves obtained with crossed nicols were found to show the same behaviour for all wave-

lengths for all thicknesses as those obtained in the case of normal pleochroic minerals. Furthermore, judging from the minimum intensity and its position, it is no doubt that the (100) section of heikolite will show complete straight extinction even for the white light.

Measurements on other sections

The intensity curves obtained for the section nearly perpendicular to [001] with the polarizer only are shown in Fig. 3. From the curves in Fig. 3, one can easily see that the absorption corresponding to the wave vibrating parallel to [010] is much stronger than that vibrating perpendicular to it.

As is observed for the (100) section, complete extinction also took place in this section under the crossed nicols.

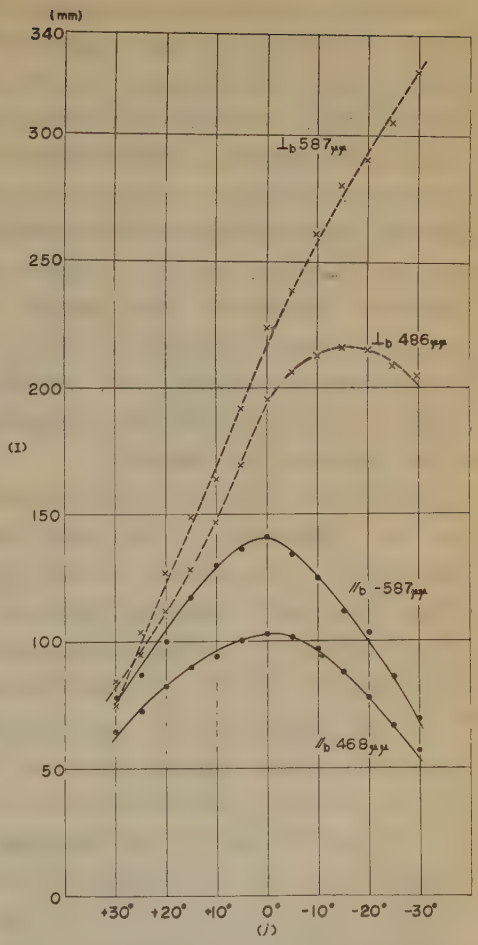

Fig. 4. The curves showing the dependence of the intensity variations on directions for the section $\rho \fallingdotseq 47°$, $\varphi \fallingdotseq 90°$.
Full lines: Vibrations parallel to [010].
Broken lines: Vibrations perpendicular to [010].
I: Scale readings on the apparatus.
j: Rotation angle about the horizontal axis of universal stage.

Owing to the difficulty of making a thin section perpendicular to [001] of heikolite, the size of the section prepared was very small (about 0.5 mm. in diameter), hence the dependence of the absorption on the direction by use of the universal stage could not be measured.

The measurements on the variation of absorption with the universal stage were also made for the section with orientation $\rho \fallingdotseq 47°$, $\varphi \fallingdotseq 90°$. The result are shown in Fig. 4. As shown in the figure, the curve obtained for the vibration perpendicular to [010] show a behaviour asymmetric with respect to the zero position. The intensity becomes stronger as [001] is approached but it decreases in the direction towards (100). On the contrary, for the vibration parallel to [010], the intensity symmetrically decreases on both side of the normal of the section.

From the behaviour of the curves obtained above, it seems probable that the absorption of the wave vibrating parallel to [010] is independent of the propagation direction of the wave in the range from the normal to (100) to [001]. On the other hand, for a wave with the vibration direction perpendicular to [010], the dependence on propagation direction is considerable.

By rotating the horizontal axis of the universal stage, we observed the intensity under crossed nicols in the direction inclining about 20° from the normal of every section above described towards [010]. On rotating the stage at that direction, it was observed that the complete extinction was obviously disturbed, in other words, the complete extinction can only be observed when the propagation direction of the wave is parallel to the (010) plane.

The section with orientation $\rho \fallingdotseq 90°$, $\varphi \fallingdotseq 50°$ does not show the complete extinction, and the direction parallel or perpendicular to [001] does not mean the direction of linear vibration. In order to see the variation of absorption when the propagation direction approaches parallel to [010] the measurements with the universal stage were also made. The results are shown in Fig. 5. As is seen from Fig. 5, the value of the absorption for the directions at right

angle to [001] increases very rapidly as the direction of propagation varies from the normal of (100) to that of (010).

Absorption ellipsoid and indicatrix

Summarizing the results obtained above as well as reported in the previous paper[2], it can be concluded that the surface showing the variation in light absorption will be symmetric with respect to the three planes namely, (010) and planes nearly parallel to (100) and nearly perpendicular to [001] respectively.

The absorption surface of the normal pleochroic crystal has been considered to be deduced from an absorption ellipsoid.* Denote by Z the direction of major axis, by X that of the minor, and by Y, intermediate, of the absorption

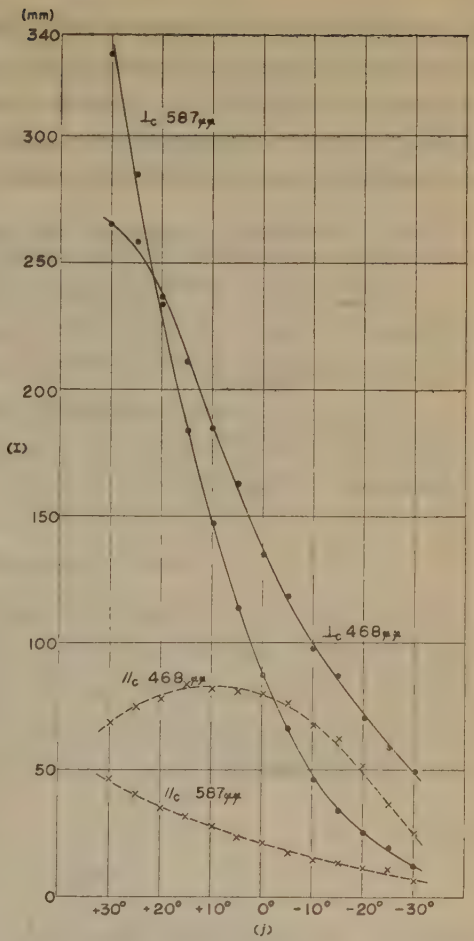

Fig. 5. The curves showing the dependence of the intensity variations on directions for the section $\rho \fallingdotseq 90°$, $\varphi \fallingdotseq 50°$.
Full lines: Cleavage trace is at right angle to the vibration direction of polarizer.
Broken lines: Cleavage trace is parallel to the vibration direction of polarizer.
I: Scale readings on the apparatus.
j: Rotation angle about the horizontal axis of universal stage.

* Pockel: Lehrbuch der Kristalloptik, p. 382.

ellipsoid, then the orientation of these absorption axes with reference to the crystallographic orientation in heikolite will be determined as shown in Table 1. The ellipsoid is very oblate in the direction of the X axis with the major axis nearly as long as the intermediate one, and becomes an ellipsoid of revolution for the definite wave

Table 1. Orientation of absorption axes and pleochroism of heikolite.

Orientation of absorption axes	Pleochroism
X nearly $\perp$(100)	
Y (Z) } $\parallel$ [010] (668 mμ, 587 mμ, 468 mμ) (501 mμ)	X...yellowish brown
Z (Y) } nearly $\parallel$ [001] (668 mμ, 587 mμ, 468 mμ) (501 mμ)	Y...deep yellowish green
	Z...deep bluish green
Absorption: $\parallel$Z > $\parallel$Y $\gg$ $\parallel$X	

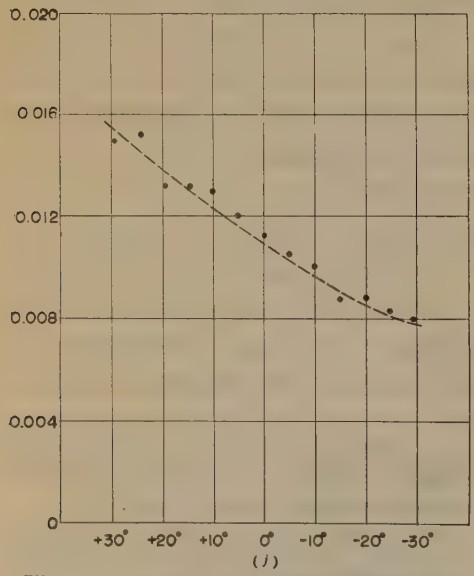

Fig. 6. The curves showing the dependence of the birefringence on direction for the (100) section of heikolite. (λ=587 mμ.)
j: Rotation angle about the horizontal axis of universal stage.

lengths of 550 mμ. or 487 mμ..

From the observations for all the section showing the complete extinction, it was shown that the waves vibrating parallel to [010] correspond always to the slower waves. Consequently the optical axes must lie in a plane perpendicular to the (010) plane.

Since the values of the absorption of one wave does not differ much from the other (both waves propagating in the same direction) for the direction not far from the normal to (100), it was possible to measure

the retardation in the (100) section by use of the compensator. By rotating the (100) section about the horizontal axis of the universal stage, the retardation of the two waves propagating to the various directions perpendicular to [010] were successively measured by the compensator. The dependence of the birefringence on direction is shown in Fig. 6.

No position which corresponds to the direction of optic axis or bisectrix could be found in this figure.

Hence, it may be concluded that in the (010) plane of heikolite the orientation of the principal axes of its absorption ellipsoid does not coincide with that of its indicatrix.

A thorough discussion on the anomalous optical behaviour of heikolite will be given in a paper to be published in near future.

Acknowledgements

The writer wishes to thank Professor T. Ito, the Institute of Mineralogy, and Professor N. Katayama, College of General Education, for their encouragements during the present work. His thanks are also due to Assistant Professor R. Morimoto and Mr. T. Watanabe, the Earthquake Research Institute, for their help in preparation of sections.

References

1) Katayama, N. and Y. Sato: Jour. Miner. Soc. Jap., 1, 73, (1953) (in Japanese).
2) Shoda, T.: Miner. Jour., 1, 69 (1954).

Manuscript received Sept. 11, 1956.

Mineralogical Journal, Vol. 2, No. 1, pp. 48-58, Dec., 1956

SHORT COMMUNICATIONS

FREQUENCY DISTRIBUTION OF THE COMPOSITION OF PLAGIOCLASES IN SOME IGNEOUS ROCKS

Teiroku Sueno

Onoda Cement Co. Ltd.

The zonal structure of plagioclases in igneous rocks has been studied by many investigators, but the data for relative abundance of each composition in the zoned plagioclases have been lacking. In order, to obtain such data the present writer measured the refractive indices in cleavage-flakes of plagioclases, picked up both from the groundmass and from the phenocrysts of the andesites, exposed in the neighbourhood of the swamp of Ozenuma, Gumma Prefecture, and in Volcano Norikura-daké, Nagano Prefecture, and also from granodiorite in the neighbourhood of the spa of Murasugi, Niigata Prefecture.

In this paper are given the statistical data of relative abundance of each composition in the zoned plagioclases, as determined from the measurement of refractive indices. Some discussions will be made on the relations between the modes of zoning of porphyritic plagioclases and the compositions of groundmass plagioclases.

Measurements

The universal stage method for determining the composition of plagioclases is inadequate for obtaining the quantitative ratio of plagioclases of different compositions, because the thin section there used is indefinitely cut both in regard to parts and directions. Ac-

cordingly, the writer picked up plagioclase phenocrysts in as perfect state as possible using fine chisels and crushed them carefully in the mortar into cleavage pieces to measure their refractive indices.

To obtain the materials from groundmass, the writer at first crushed a piece of groundmass free from phenocrysts into powders finer than in the case of phenocryst, and selected clear cleavage pieces under crossed nicols.

S. Tsuboi's dispersion method[2)3)4)5)] for determining plagioclases in cleavage-flakes was applied throughout the measurements. The results obtained are shown in Figs. 1~3, giving the frequency distribution of compositions taken at intervals of one per cent Ab.

The number of cleavage-flakes measured was about two hundred for each crystal from the granodiorite of Sugimura, while it was about sixty for phenocrysts from volcanic rocks.

Results

(1) *Plagioclases in the andesite in the neighbourhood of the swamp of Ozenuma**. (Fig. 1)

The present writer previously reported[1)] the composition of plagioclase phenocrysts in the andesite in the neighbourhood of the swamp of Ozenuma on the boundary between Gumma and Fukushima prefectures. The ranges of their compositions are as shown in Table 1 and in Fig. 1.

The frequency distribution of the compositions of the groundmass feldspars reveals that there is a considerable range even within a small piece of specimen, at variance with the general expectation that groundmass plagioclases would be of nearly uniform composition. The wide compositional range of the groundmass plagioclases here observed may be attributed to the viscosity of the Ozenuma lava flows.

Other facts to be noticed are: that in several cases there are two

* 尾瀬沼

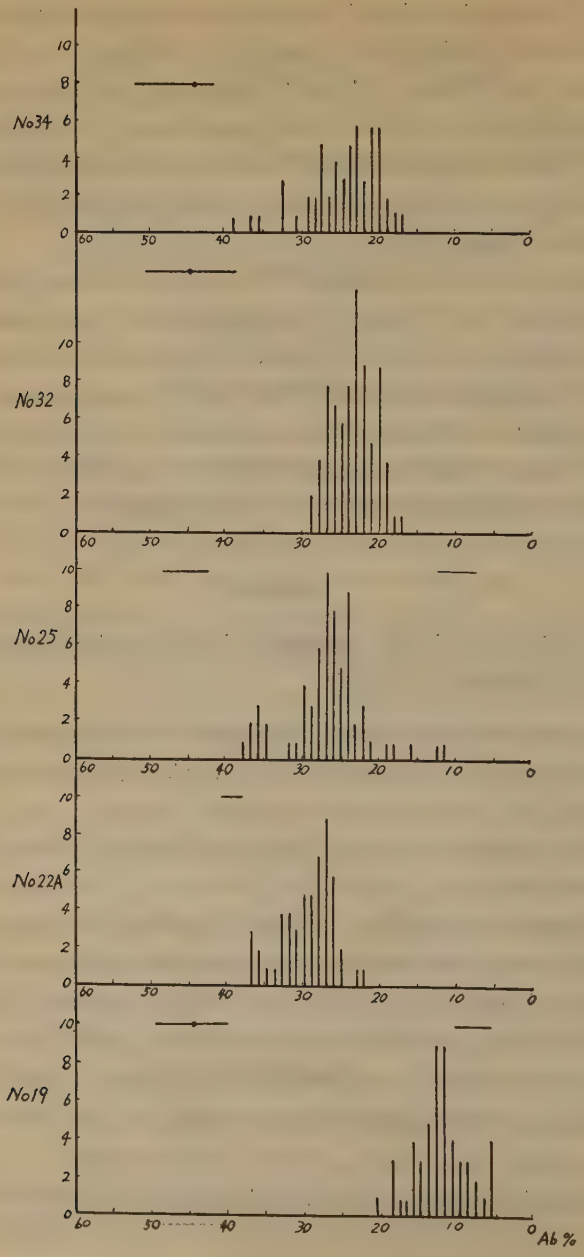
No34
No32
No25
No22A
No19
0
2
4
6
8
10
60
50
40
30
20
10
0
Ab %

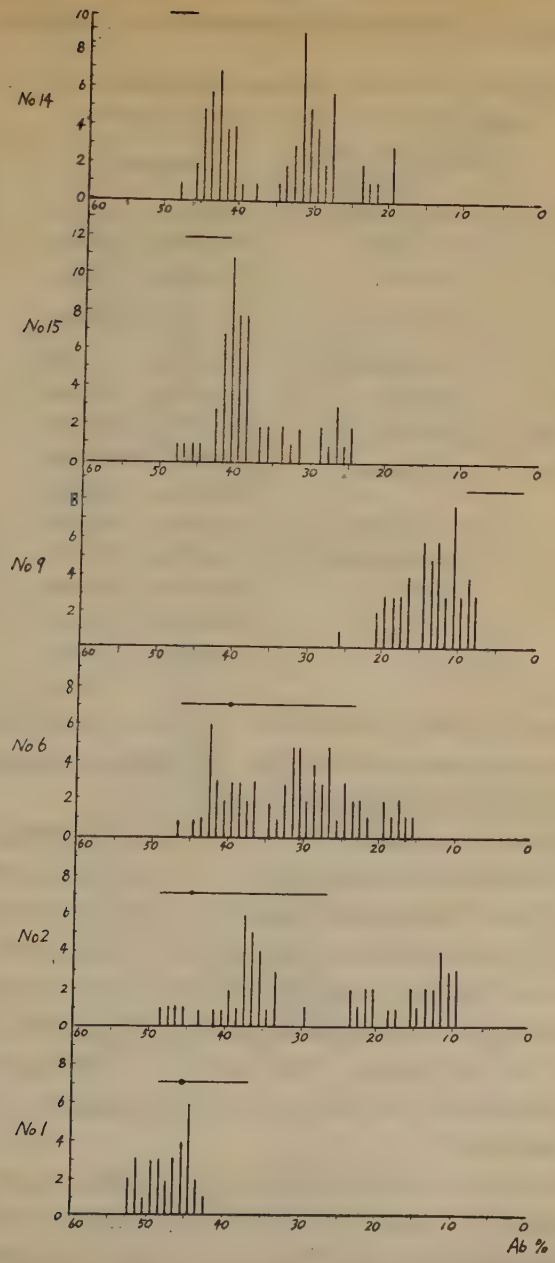

Fig. 1. Frequency distribution of the composition of plagioclases in the andesites from Ozenuma region.
No. 's refer to those in Table 1.
Lateral lines represent the range of composition of plagioclase phenocrysts.

Table 1. Composition of the plagioclase phenocrysts of andesites in the neighbourhood of the swamp of Ozenuma.

Specimen	Number of crystals measured	Composition	The most common
Hiuchidaké 32	5 phenocrysts.	$Ab_{51}An_{49}-Ab_{39}An_{61}$	$Ab_{45}An_{55}$
Hiuchidaké 34	5~6 phenos.	$Ab_{52}An_{48}-Ab_{42}An_{58}$	$Ab_{45}An_{55}$
Keikakusan 26	2 phenos.	$Ab_{43}An_{57}-Ab_{39}An_{61}$	
Southern foot of Hiuchidaké 15	5~6 phenos.	$Ab_{47}An_{53}-Ab_{41}An_{59}$	
Fujimi pass 6	5~6 phenos.	$Ab_{47}An_{53}-Ab_{24}An_{76}$	$Ab_{40}An_{60}$
Fujimi pass 9	1 pheno.	$Ab_{7}An_{93}-Ab_{1}An_{99}$	
Hidakayama 22A	1 pheno.	$Ab_{41}An_{59}-Ab_{39}An_{61}$	
Hidakayama 25	5~6 phenos.	$Ab_{49}An_{51}-Ab_{43}An_{57}$ $Ab_{12}An_{88}-Ab_{7}An_{93}$	
Shore 1	5~6 phenos.	$Ab_{49}An_{51}-Ab_{37}An_{63}$	$Ab_{45}An_{55}$
Shore 2	Whole plagio.	$Ab_{49}An_{51}-Ab_{27}An_{73}$	$Ab_{45}An_{55}$
Shore 16	1 pheno.	$Ab_{49}An_{51}-Ab_{47}An_{53}$	
Shore 19	5~6 phenos.	$Ab_{50}An_{50}-Ab_{40}An_{60}$ $Ab_{10}An_{90}-Ab_{5}An_{95}$	$Ab_{45}An_{55}$

maxima in the frequency distribution of the compositions of the groundmass plagioclases, and that the groundmass plagioclases are often more calcic than porphyritic ones.

In some cases, as exemplified by No. 34, many plagioclase phenocrysts have reversed zonal structure, with distinctly bordered outer zone of more calcic composition than the inner one. In such cases, plagioclases in groundmass are always more calcic than those of phenocrysts, and the most calcic part of the latter is of nearly the same composition as the most sodic part of the groundmass plagioclases. This may be taken as showing that in the course of the growth of these phenocrysts there occurred repeatedly additions of some basic magmas.

In some rocks, as No. 6 for example, both ordinary and reversed zonal structures are seen in plagioclase phenocrysts. Then, the groundmass plagioclases are of nearly the same compositions with the porphyritic ones.

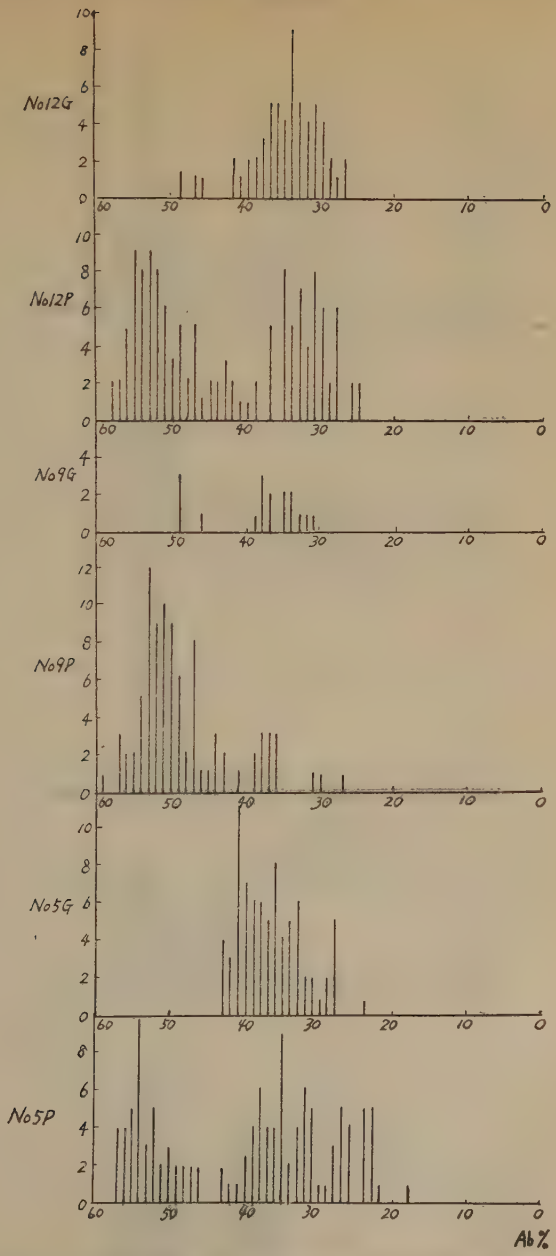

Fig. 2. Frequency distribution of the composition of plagioclases in the andesites from Norikura-daké.
G: groundmass, P: phenocryst.

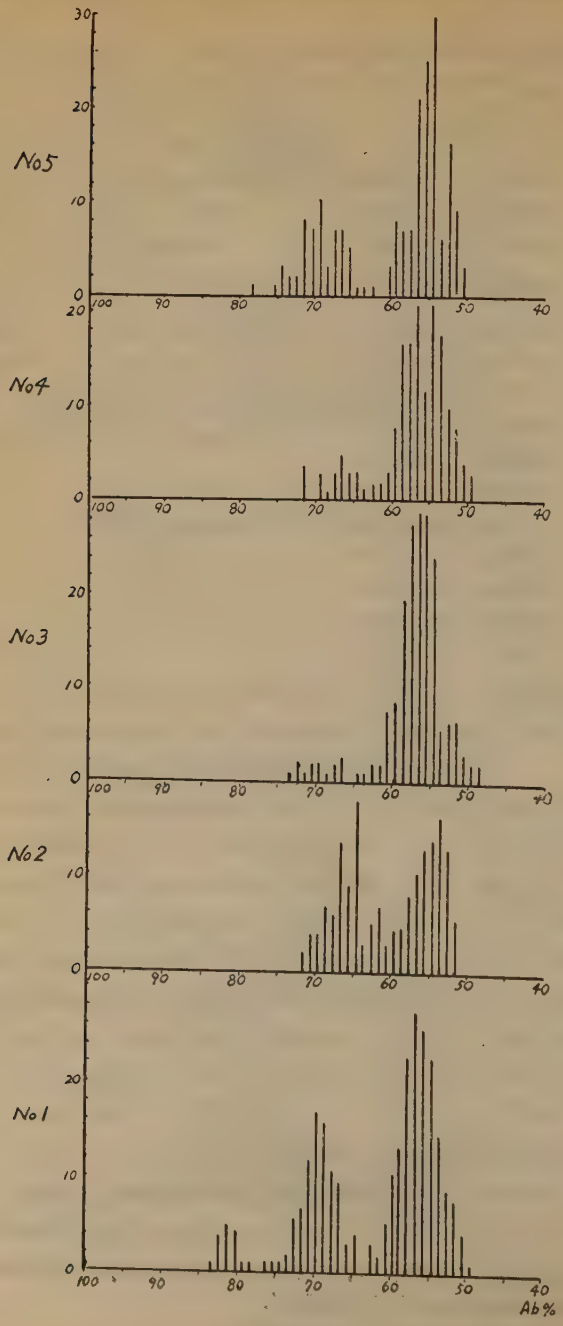
No5
No4
No3
No2
No1
0
10
20
30
100
90
80
70
60
50
40
Ab%

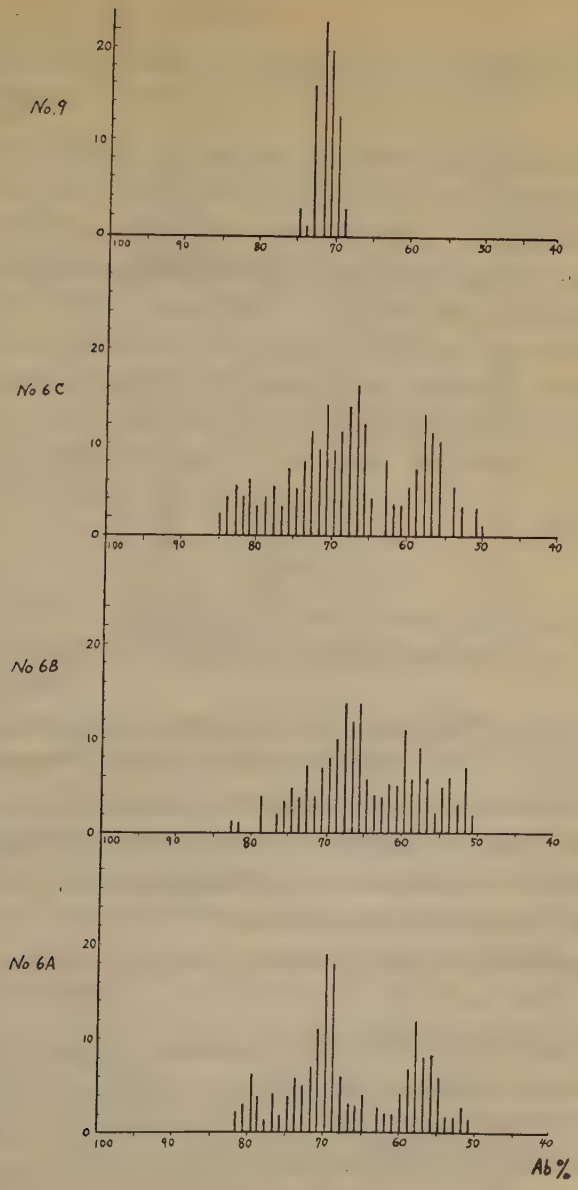
No. 9
No 6 C
No 6B
No 6A
20
10
0
100
90
80
70
60
50
40
Ab %

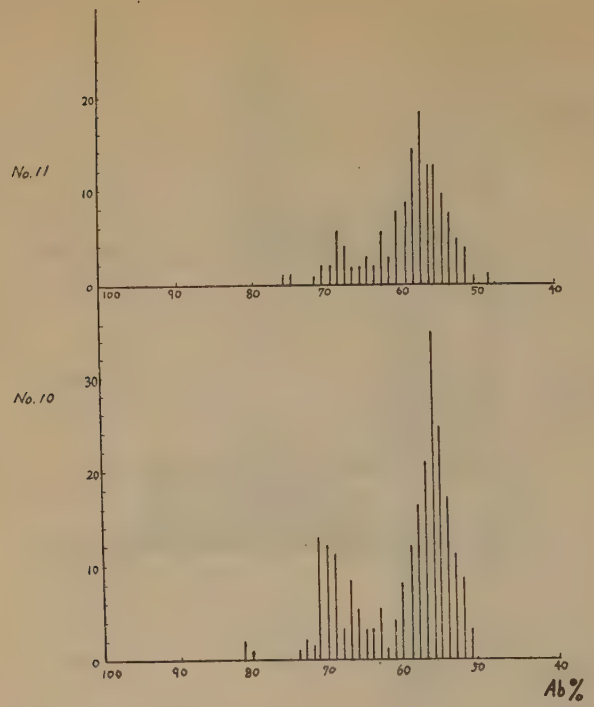

Fig. 3. Frequency distribution of the composition of plagioclases in the granodiorite in the neighbourhood of the spa of Murasugi.

Some specimens, such as No. 25 and No. 19, have plagioclase phenocrysts of two distinct compositions. Then, the range of composition of the groundmass plagioclase is a little more sodic than that of the more calcic plagioclase phenocrysts.

(2) *Plagioclases in the andesite of Volcano Norikura-dake**. (Fig. 2)

The compositions of grouudmass plagioclases are distributed through a considerable range, as in the case of Ozenuma. The frequency distribution of the compositions of phenocrysts distinctly shows two maxima, the more calcic one of the two being slightly more calcic

* 乗鞍岳

than the groundmass plagiocalses.

(3) *Plagioclases in the granodiorite in the neighbourhood of the spa of Murasugi**. (Fig. 3)

In the neighbourhood of the spa of Murasugi, Nakakanbara-gun, Niigata Prefecture, there occur several types of granodiorite with different aspects. Generally the frequency distribution of the compositions of their plagioclases shows two maxima, one at about Ab_{55} and the other at about Ab_{70}. The former maximum is more dominent than the latter with distinct minimum between them at about Ab_{65} in the case of the granodiorite containing pale fleshred orthoclase, while in the case without such coloured orthoclase (No. 6 in Fig. 3) the maxima appear to be rather obscure and the whole range of distribution is considerably broad.

Summary

As the materials used for this study are of common type, the results obtained may be considered to represent some general relations.

The frequency distribution of the compositions in each plagioclase crystal occurring as a component of granodiorite or as phenocrysts of andesite shows generally one maximum or two (Figs. 2 and 3).

The groundmass plagioclases of andesites have been found not to be uniform in their composition even within one sheet of lave. The range of their composition attains to forty per cent Ab, and has an intimate relation with the mode of zoning of the coexisting plagioclase phenocrysts. The viscosity of the lava flow in which the plagioclases were formed may be a controling factor for their compositional distribution.

In conclusion the writer wishes to express his gratitude to Dr. Seitaro Tsuboi, Emeritus Professor of University of Tokyo, for his encouragement of this research.

---

* 村杉温泉

References

1) Sueno, T.: Rept. Natural Monument Surv., (1933) (in Japanese).
2) Tsuboi, S.: Min. Mag., **20**, 108 (1923).
3) Tsuboi, S.: Jour. Geol. Soc. Tokyo, **32**, 1 (1925).
4) Tsuboi, S.: Jour. Fac. Sci. Imp. Univ. Tokyo, Sec. II, Pt. 5, **1**, 139 (1926).
5) Tsuboi, S.: Jour. Geol. Soc. Tokyo, **37**, 39 (1930).

Manuscript received Sept. 15, 1956.

ABSTRACT OF THE KOBUTSUGAKU ZASSHI, JOURNAL OF THE MINERALOGICAL SOCIETY OF JAPAN, VOL. 3, NO. 1, October, 1956

On the Solubility of Ionic Salts (pp. 1—9)

Masaru Goto

When crystals are in their water solutions, the bond energy U_0 of the constituent ion on the crystal surface corresponds to the difference between crystal energy and heat of hydration. For the simple crystal types of M^+-X^- and $M^{++}-X^{--}$, attempts of introducing an equation which evaluates U_0 yield to give the result shown as follows:

$$U_0=\frac{1}{2}A_{R0}e^2/(R_1+R_2)$$
$$-[N_1z_1e\mu/(R_1+1.65)-N_1z_2e\mu/(R_2+2R_1+1.65)^2]$$
$$-[N_2z_2e\mu/(R_2+1.15)-N_2z_1e\mu/(R_1+2R_2+1.15)^2],$$

where A_{R0} denotes the Madelung constant, z the electric charge of ion, R the ionic radii, N the number of water molecules coordinated to each ion, and the suffix 1 and 2 denote the positive and negative ions respectively. In the case of alkali halides, the writer obtained a smooth increasing curve representing the relation between the observed solubilities and $(-U_0)$ assigning $N_1=N_2=4$, and deduced from it that the heat of hydration U_h of Cs^+ has nearly the same value with that of J^-. The values of the heat of hydration of alkali and halogen ions thus obtained are as follows;

Li^+	123.4 kcal/g. ion	F^-	112.3 kcal/g. ion
Na^+	99.3	Cl^-	80.1
K^+	78.6	Br^-	73.2
Rb^+	71.2	J^-	64.0
Cs^+	64.8		

Studies on Manganese Ores (I), *Determination of Quartz Content* (pp. 10—19)

Takuya Imai and Harumichi Kaneko

Mineral constituents of manganese ores considerably affect the process of producing ferro alloys. The writers intended to determine the constituent minerals by means of chemical analysis.

In the first place, we examined the method of quantitative determination of quartz crystal in the ores. Using the principle of Talvite method, and taking rock crystal and rhodonite as standard samples, the writers obtained good results under the following conditions; size grade of material: −200 mesh, heating of phosphoric acid: at 280°~290°C. for about 15 min.. The quartz content we obtained was 0.7% for sample I (an ore for high carbon ferro-manganese, Mn 46%, SiO_2 15%), and 49.8% for sample II (an ore for silico-manganese, Mn 20%, SiO_2 60%). These results were confirmed by X-ray method.

On the Pyromorphite-Mimetite Series Found in Japan (Rept. 2) (pp. 20—31)

Kunihiko Muta

Relations between minor components and crystal habit, colour and also types of ore deposits were examined for the minerals of pyromorphite series.

In general, red or violet-brown varieties are characterized by large x faces, and are richer in Cu, V or Ca, poorer in Fe, than yellow or green varieties. Those components appear to affect the colour or crystal habit of the crystals of this series. The varieties and contents of the minor components in this series reflect the characteristcs of its original deposit, hence they will contribute to the estimation of the genesis of ore deposit or to the consideration of mineral provinces.

The minor elements, which are more abundant in pyromorphite series than in the galena or other primary minerals in its original deposit, are restricted to those which have an ionic radius similar to one of the main components of the series or to those whose ionic potential is lower than 3 or higher than 12.

Dielectric Dispersion of Allanite (pp. 32—38)

Satoru Kakitani

The dielectric dispersion of allanite from Manchuria was confirmed to take place at about 450°C. in the frequency region between 100 kc. and 5 Mc.. Taking into consideration the results of X-ray investigation, differential thermal

analysis and measurement of direct current conductivity, the writer concluded that the cause of the dielectric dispersion in this case may be attributed to the recrystallization of partly metamict mineral.

The Debye patterns of the quenched materials from 370°C., 500°C., 620°C., 700°C. and 1,000°C. were studied for allanites from Manchuria and Daimonji-yama. The patterns of the former considerably change between room temperature and 700°C. until they become similar to those of the latter which do not show any noticeable difference up to 700°C.. The patterns of the materials quenched from 1,000°C., irrespective of their locality, consist of the lines of hematite and several unidentified ones which probably due to the thermal decompostion of allanite.

The lattice constants of the allanite from Daimonjiyama determined by oscillation method are as follows;

	a_0	b_0	c_0	β
Not heated	8.84 Å	5.73 Å	10.25 Å	115°05′
Quenched from 840°C	8.83	5.62	10.50	117 30

The conductivity versus $1/T$ diagram consists of three straight lines with two bent points at 655°C. and 1,030°C.. The activation energies calculated from these data are as follows; $E_1=0.81$ eV. (575°~655°C.), $E_2=1.00$ eV. (655°~1,030°C.) and $E_3=11.7$ eV. (>1,030°C.).

On the Growth Relations of Orthoclase and Adularia from Banda, Tôji-Machi, Okayama Prefecture (pp. 39—48)

Takeshi Tomisaka, Kitinosuke Henmi and Goro Shibuya

Crystals of orthoclase overgrown with adularia were collected from a pegmatite in biotite-granite at Banda, Tôji-machi, Okayama Prefecture. The crystal habit of the orthoclase is variable, the most abundant being Baveno or Manebach twins elongated along [100], while the overgrowing adularia displays its characteristic habit with dominant *x* and *m* faces. Successive change in the course of crystallization of adularia was revealed.

The composition of the orthoclase was determined as $Or_{65}Ab_{33}An_2$ and that of the adularia as $Or_{86}Ab_{11}An_3$. The crystallization temperature of the former was estimated to be about 590°~600°C., and that of the latter 380°C.,

after Barth's diagram. Taking into consideration the distinct gap between these temperatures as well as the sharp boundary between the crystals of orthoclase and overgrown adularia, the writers inferred that some hydrothermal solution ascended into the pegmatite after its solidification and brought about the overgrowth of adularia upon pre-existing orthoclase.

Short Communications

Studies on Infrared Absorption for Some Clay Minerals (On the OH-stretching Vibration of Montmorillonite, Kaolinite and Halloysite, Supplement) (pp. 49—52)

Satoru Kakitani

The infrared absorption spectra due to OH radical ranging from 2.4 to 3.0 μ. has been provided for identification of the heading minerals. The absorption by montmorillonite at 2.76 μ. may be interpreted as the absorption due to the OH radical and those at 2.8~3.0 μ. due to the interlayer H_2O molecule, the former resembling to the absorption by the OH radical of muscovite. When montmorillonite is heated for five hours in 5 mm. Hg vacuum, the broad absorptions between 2.8 μ. and 3.0 μ. almost disappear, while the sharp absorption at 2.76 μ. disappears at about 810°C.. Both kaolinite and halloysite show the absorptions due to their two sorts of OH radicals at 2.76 μ. and 2.71 μ. respectively, but these characteristic absorptions disappear when the minerals are heated at 700°C..

Reviews

Mineral Composition of Limonite.....Matsuo Nambu... 53—76
Proceedings..... 81—106

Mineralogical Society of Japan

OFFICERS FOR 1956–1957

President: Teiichi Ito, University of Tokyo, Tokyo.

Vice-President: Bumpei Yoshiki, Asahi Glass Co. Ltd., Tokyo.

Secretary: Toshio Sudo, Tokyo University of Education, Tokyo. Keiichi Omori, Tohoku University, Sendai.

Treasurer: Tokugoro Shoda, University of Tokyo, Tokyo.

Editor: Nobuo Katayama, University of Tokyo, Tokyo.

Councillors: Zyunpei Harada, Masao Ishibashi; Hokkaido University, Sapporo. Keiichi Omori, Tsunehiko Takeuchi; Tohoku University, Sendai. Teiichi Ito, Shuichi Iwao, Nobuo Katayama, Eiichi Minami, Tokugoro Shoda, Seitaro Tsuboi, Takeo Watanabe; University of Tokyo, Tokyo. Toshio Sudo, Tokyo University of Education, Tokyo. Teiroku Sueno, Onoda Cement Co. Ltd., Tokyo. Bumpei Yoshiki, Asahi Glass Co. Ltd., Tokyo. Kin-ichi Sakurai, Tokyo. Yasuo Ukai, University of Kyoto, Kyoto. Ryoiti Kiriyama, University of Osaka, Osaka. Yoshio Kinosaki, Hiroshima University, Hiroshima. Kameki Kinoshita, Toyofumi Yoshimura; Kyushu University, Fukuoka.

PUBLICATIONS

Kôbutsugaku Zasshi, Journal of the Mineralogical Society of Japan

A journal containing articles and reviews on mineralogy and allied sciences contributed by members of the Mineralogical Society of Japan. Published every four months, in Japanese. Sent to all members of the Society. Membership dues $2.00 annually.

Mineralogical Journal

A journal containing articles on mineralogy and allied sciences, published semi-annually in English principally. Contributions are invited from everyone.

The Journal completed its first volume of six numbers in 1956. Back numbers may be obtained at $1.00 per single copy for the time being. The price of subsrciption to the second volume is $5.00 per volume.

Printed by "HERALD" Printing Co., Ltd.